Journal of Mechanics of Materials and Structures

A NUMERICAL MODEL FOR MASONRY-LIKE STRUCTURES

Maurizio Angelillo, Luca Cardamone and Antonio Fortunato

Volume 5, No. 4

April 2010

A NUMERICAL MODEL FOR MASONRY-LIKE STRUCTURES

MAURIZIO ANGELILLO, LUCA CARDAMONE AND ANTONIO FORTUNATO

Masonry has historically been one of the most widely used construction materials. Despite this, there is a lack of computational tools for the analysis of masonry structures compared with what is available for steel and concrete structures. One of the main reasons is likely to be found in the peculiar mechanical behavior of masonry, which shows a small and unpredictable resistance in tension and a nonlinear inelastic behavior in compression. In this paper we put forward a constitutive model for masonry based on the extension to associate path-dependent plasticity of the classical normal, elastic, no-tension model. This new model allows the onset of fracture and irreversible crushing of the material and accounts for a wider variety of stress states within the structure, highlighting the progress of pseudorigid kinematics. The elastoplastic problem is decomposed into a sequence of nonlinear elastic problems formulated in variational form, which are solved by searching for the minimum of a suitable functional via descent methods. The model is implemented in variational finite element code and validated against analytical solutions and experimental tests. Applications to realistic cases are presented showing the capability of the model to reproduce nontrivial cracking and crushing patterns.

1. Introduction

Masonry structures, if not dry, are formed by individual blocks bound together by mortar joints. The complexity of the mechanical response of masonry materials depends not only on the narrow limits of applicability of simple theories, but above all on the inherent difficulties in the accurate characterization of their material behavior: besides the quality of the units and of the mortar, the quality of workmanship and the pattern the blocks are put in can strongly affect the mechanical properties of the overall construction in a practically unpredictable way. Although it is perfectly legitimate and appropriate to study and propose sophisticated models based on detailed knowledge of the microstructure [Luciano and Sacco 1997; Sab 2003] the range of applicability of such models is restricted to special situations. The material behavior of real masonry is strongly dependent on elastic nonlinearity, anisotropy, and friction, but considerations of simplicity and the inherent difficulties in actually knowing the material microstructure in old masonry suggest that we should not insist on very detailed descriptions of the stress-strain behavior [Lucchesi et al. 1996]. Concerning elastic nonlinearity and anisotropy there are no difficulties, at least in principle, to including such behaviors in the present model. But a reasonable model for masonry with a wide scope should be necessarily simplified and confined to the overall description of the mechanical behavior of large masonry masses.

Masonry material is brittle and characterized by a very small and unpredictable value of toughness; cracks are physiological in masonry, and are likely to open up in the material solely under the effect of working loads. As a first approximation of this behavior, a no-tension material model has been proposed.

Keywords: masonry, descent methods, energy minimization, unilateral materials, plasticity.

This crude model, which describes the material as elastic in compression but incapable of sustaining tensile stresses, was first introduced explicitly in [Heyman 1995]; however, the idea of a no-tension material underlies, more or less consciously, the design of all masonry structures, and has done so since antiquity [Benvenuto 1991], particularly in the case of vaulted structures and arches. Based on the no-tension model, the safety of the structure is a problem of geometry rather than of material strength, in keeping with the spirit of the rules of proportions used by ancient architects in masonry design. The approach of Heyman was aimed at collapse analysis of masonry structures. Analyzing the structure before collapse requires a description of strain more detailed than that considered by Heyman.

The unilateral constraint on stress produces a latent part of strain (anelastic strain) representing a local measure of cracking. A proper constraint principle has to be introduced to define the restrictions on the anelastic strain. The most popular choice is the normal elastic no-tension model (NENT) introduced in the 1980s (see [Romano and Romano 1979; Di Pasquale 1984; Castellano 1988; Angelillo 1993; Angelillo and Rosso 1995] for more general assumptions on fracture strains) and studied rigorously from the mathematical point of view in [Giaquinta and Giusti 1985]. A lucid and complete synthesis of the NENT model is presented in [Del Piero 1989].

Essentially the constitutive restrictions defining NENT materials are as follows:

– The stress tensor is assumed to be negative semidefinite and depend linearly upon the elastic part of the strain.

– The total strain is the sum of its elastic and anelastic parts.

– The anelastic strain is assumed to be normal to the boundary of the elastic stress domain and turns out to be positive semidefinite.

The NENT model gives a rather primitive description of the actual masonry behavior and can furnish only a gross overall description of the stress and fracture distribution in the material. Yet, in spite of its simplicity, it poses serious numerical problems even in the most elementary cases. A long series of papers on numerical techniques for the analysis of no-tension problems (see for example [Romano and Sacco 1984; Alfano et al. 2000] and references therein) has not, so far, produced computer codes simple enough to be included in structural analysis commercial packages. Besides, in many cases of practical interest, the structural crisis is due to simultaneous crack opening and crushing, that is, to the attainment of the limit strength in compression: the shear strength of a masonry wall depends sensibly on the crushing strength. A strength criterion in compression has to be added to the NENT model to account for such phenomena.

Here we consider a material model for masonry, called a masonry-like (ML) model, obtained by adding to the NENT restrictions a Drucker–Prager type yield criterion in compression and considering a flow rule for the corresponding anelastic strain rates of the associated type. The extension of the NENT model to limited compressive strength was considered in [Lucchesi et al. 1996; Marfia and Sacco 2005]. Both numerical approaches require the computation of the tangent stiffness matrix in order to determine the solution of the equilibrium problem. The ML material with bounded compressive strength proposed in [Lucchesi et al. 1996] is basically an elastic (i.e., conservative) NENT model with nonlinear behavior in compression, and therefore does not account for irreversible crushing and energy dissipation in the material. The model proposed in [Marfia and Sacco 2005] accounts for irreversible crushing of the material using a complex return mapping algorithm to compute the plastic strains.

The main contributions of the present paper consist in the development of an alternative numerical procedure based on descent minimization to solve the equilibrium problem at each loading step and a direct computation of the plastic strain increment, providing a simple and efficient tool for handling no-tension materials such as NENT and ML materials. The numerical method we propose, based on the NENT and ML material models, is aimed at description of the stress, fracture, irreversible crushing strain, and energy dissipation in plane masonry structures under working conditions, that is, away from collapse. This kind of analysis could be relevant in the diagnosis of structural disarrangement, where investigation is usually pursued long before signs of incipient collapse. The structure safety margins with respect to collapse can be evaluated beforehand by employing the tools of limit analysis [Como and Grimaldi 1985; Como 1992]. The presently proposed method of analysis can be applied to study collapse situations as limit cases, as illustrated by some of the examples presented in the applications.

In the first part of the paper we test the ability of our numerical approach to represent the behavior of structures made of normal elastic no-tension (NENT) material, that is, without the additional hypothesis of limited strength in compression. As proved in [Del Piero 1989] the NENT material is hyperelastic, the material response is path independent, and the equilibrium solutions can be characterized as minimizers of the total potential energy functional. Our research group in the last ten years has developed considerable numerical and computational experience in minimization problems for complex energy functionals [Angelillo et al. 2006; 2008]. The numerical technique we employ, based on descent methods (steepest descent, conjugate gradient), is unusual in structural mechanics. The convenience of descent methods, favored in recent years due to the increase of available computational power, is recovered in the case of nonsmooth energy shapes. In the specific case of masonry the method is particularly indicated since the problem becomes unconstrained and the potential energy is a convex function of its arguments. Several numerical tests we performed on simple problems, for which the exact solutions are known, show the competitiveness of the descent approach with respect to more classical techniques. Some of these benchmark problems are reported in Section 3. Comparisons with numerical solutions obtained by other developing codes [Lucchesi et al. 2008a] and commercial programs (ABAQUS) indicate [Angelillo et al. 2010] that the descent method seems to be the right choice to overcome the difficulties which are inherent to the no-tension constraint.

In the second part of this paper we consider ML materials, that is, we add to the NENT model a crushing strength criterion, considering an elastoplastic associate behavior. At first glance it seems that the proposed numerical technique, based on energy minimization (extremely convenient for unilateral materials) should be abandoned. The elastoplastic behavior is indeed inherently path-dependent: the stress state at time t depends, in general, on the whole strain history in the interval $[0, \bar{t})$ rather than on the strain at time t. Then the equilibrium problem for such a material is essentially an evolutive problem whose solution cannot be obtained by simply minimizing an energy functional. The proposed technique can still be applied to this evolutive problem considering the exact evolution as the limit of a sequence of minimum problems. This is done by discretizing the time interval into steps and updating the energy in a suitable way. The evolutive problem is then approximated as a sequence of a discrete number of minimizing movements. The evolutive solution is obtained as the limit of the discrete evolution by letting the time step go to zero (see [De Giorgi 1996] for the general formulation, and [Dal Maso et al. 2006; Mielke and Ortiz 2008] for the convergence proofs in the general case of rate independent materials and in the specific case of perfect elastoplasticity). Finally, we present some numerical results for ML structures.

2. Methods

2A. *The equilibrium problem for NENT materials.*

2A1. *Minimum problem.* Many problems in mathematics and physics can be formulated in terms of a minimum search: a functional describing the energy of the system and depending on an unknown function has to be minimized over the set of all admissible functions.

The form of energy to be minimized in the case of NENT materials is

$$\mathcal{E}(\boldsymbol{u}) = -\int_{\partial\Omega_N} \boldsymbol{p} \cdot \boldsymbol{u}\,ds - \int_{\Omega} \boldsymbol{b} \cdot \boldsymbol{u}\,da + \int_{\Omega} \varphi\big(\boldsymbol{e}(\boldsymbol{u})\big)\,da, \tag{2-1}$$

where $\boldsymbol{p}$ and $\boldsymbol{b}$ are the given loads, $\boldsymbol{e}(\boldsymbol{u})$ is the infinitesimal strain associated to $\boldsymbol{u}$:

$$\boldsymbol{e}(\boldsymbol{u}) = \tfrac{1}{2}(\nabla\boldsymbol{u} + \nabla\boldsymbol{u}^{\mathrm{T}}), \tag{2-2}$$

and $\varphi\big(\boldsymbol{e}(\boldsymbol{u})\big)$ is the elastic energy density. Then the stress $\boldsymbol{T}$ is related to $\boldsymbol{e}$ through the relation

$$\boldsymbol{T} = \frac{\partial\varphi}{\partial\boldsymbol{e}}. \tag{2-3}$$

The minimizer of $\mathcal{E}(\boldsymbol{u})$ is searched for as $\boldsymbol{u} \in \mathscr{S}$ (a Banach space) and $\boldsymbol{u} = \bar{\boldsymbol{u}}$ on $\partial\Omega_D$, where $\bar{\boldsymbol{u}}$ is the given displacement. The nature of such a Banach space and other results concerning the principle of minimum potential energy and the minimum of complementary energy are discussed in Appendix A.

2A2. *The boundary value problem in two dimensions.* As shown in [Del Piero 1989], an energy form $\varphi\big(\boldsymbol{e}(\boldsymbol{u})\big)$ can be introduced such that the minimum problem for the functional (2-1) provides the existence of the solution for the following boundary value problem in the two-dimensional case:

Given a bounded open set Ω of $\mathbb{R}^2$ and given

$$\boldsymbol{p} : \partial\Omega_N \to V^2, \quad \boldsymbol{b} : \Omega \to V^2, \quad \bar{\boldsymbol{u}} : \partial\Omega_D \to V^2, \tag{2-4}$$

find the fields

$$\boldsymbol{u} : \Omega \to V^2 \quad \text{and} \quad \boldsymbol{T} : \Omega \to \mathrm{Sym} \tag{2-5}$$

such that

$$\boldsymbol{T} \in \mathrm{N\,Sym} \ \text{ for } \boldsymbol{x} \in \Omega, \quad \boldsymbol{e}(\boldsymbol{u}) = \boldsymbol{\varepsilon} + \lambda, \quad \boldsymbol{\varepsilon} = \mathbb{A}[\boldsymbol{T}], \quad \lambda \in \mathrm{P\,Sym} \ \text{ for } \boldsymbol{x} \in \Omega, \quad \boldsymbol{T} \cdot \lambda = 0, \tag{2-6}$$

where N Sym and P Sym are the closed cones of negative semidefinite and positive semidefinite symmetric second order tensors and $\mathbb{A}$ is the positive definite fourth-order tensor of the elastic compliances, such that

$$\operatorname{div}\boldsymbol{T} + \boldsymbol{b} = \boldsymbol{0} \ \text{ in } \Omega, \quad \boldsymbol{T}\boldsymbol{n} = \boldsymbol{p} \ \text{ on } \partial\Omega_N, \quad \boldsymbol{u} = \bar{\boldsymbol{u}} \ \text{ on } \partial\Omega_D, \tag{2-7}$$

$\boldsymbol{n}$ being the unit outward normal to Ω.

The mechanical interpretation of conditions (2-6) and (2-7) is as follows. Conditions (2-6) are the restrictions characterizing NENT materials. They state that the stress $\boldsymbol{T}$ is negative semidefinite, that is,

$$\boldsymbol{T} \cdot \boldsymbol{m} \otimes \boldsymbol{m} \leq 0 \ \text{ for } \boldsymbol{m} \in V^2 \qquad \text{(no-tension assumption)}. \tag{2-8}$$

The total strain $\boldsymbol{e}$ is the sum of two parts: an elastic part $\boldsymbol{\varepsilon}$ related to the stress $\boldsymbol{T}$ through the linear operator $\mathbb{A}$ and a latent anelastic part λ which is positive semidefinite and orthogonal to $\boldsymbol{T}$. Conditions

(2-7) correspond to the equilibrium balance at the interior and on the part $\partial \Omega_N$ of the boundary, with the given force fields b and p, and to the compatibility of the displacement field with the displacement given on the part $\partial \Omega_D$ of the boundary.

Notice that the condition on the displacement should actually be unilateral, since the material can open up freely. A way to keep the same displacement boundary conditions of classical elasticity is to consider the domain Ω closed on $\partial \Omega_D$, that is, to add to the domain a one-dimensional skin that must comply with the constraint on displacement, and to allow for concentrated deformations on $\partial \Omega_D$.

2A3. *Fundamental partition of a no-tension body.* The no-tension hypothesis restricts the stress to belonging to the cone of negative semidefinite symmetric tensors N Sym. This restriction is equivalent to restricting the principal stresses to be nonpositive. In the two-dimensional case the no-tension assumption is also equivalent to imposing the following restrictions on the invariants of T:

$$\operatorname{tr} T \leq 0 \quad \text{and} \quad \det T \geq 0. \tag{2-9}$$

These inequalities lead naturally to the following partition of the domain Ω:

$$\begin{aligned}
\Omega_1 &= \{x \in \Omega : \operatorname{tr} T < 0, \det T > 0\}, \\
\Omega_2 &= \{x \in \Omega : \operatorname{tr} T < 0, \det T = 0\}, \\
\Omega_3 &= \{x \in \Omega : \operatorname{tr} T = 0, \det T = 0\}.
\end{aligned} \tag{2-10}$$

In Ω_1 the material subject to biaxial compression and behaves as a classical bilateral elastic material; in Ω_3 it is completely inert while in Ω_2 it is under uniaxial compression. Notice that in Ω_2 the equilibrium equations and the condition $\det T = 0$ form a system of three equations in the three unknown independent components of T. The differential problem is parabolic and the stress is determined by equilibrium regardless of the material response. In Ω_1 fractures are not possible, that is, $\lambda = 0$. In Ω_3, where $T = 0$ any positive semidefinite fracture field is possible. Also in Ω_2 the material can be fractured. The necessity of fractures is naturally produced by the problem being statically determined: the elastic strain associated with the statically determined stress is generally not compatible and fracture strains are required to restore compatibility.

The normality condition requires that in Ω_2 the fractures must open up orthogonally to the isostatic lines of compression. In an orthogonal curvilinear frame with natural bases $\{a_1, a_2\}$ coincident with the eigenvectors of T, T admits the representation

$$T = \sigma \frac{a_1 \otimes a_1}{a_1 \cdot a_1}, \tag{2-11}$$

with σ the only nonzero, negative eigenvalue of T. Normality implies the following form for the fracture strain λ:

$$\lambda = \lambda \frac{a_2 \otimes a_2}{a_2 \cdot a_2}, \tag{2-12}$$

where λ is the only nonzero, nonnegative eigenvalue of λ. Then regardless of the elastic anisotropy of a NENT material the principal directions of stress and anelastic strain are always coincident all over Ω.

2A4. *The strain energy density in two dimensions.* In the one-dimensional case the behavior of NENT materials is summarized by the stress-strain graph of Figure 1. Notice that the stress-strain relation is completely reversible both in traction and compression.
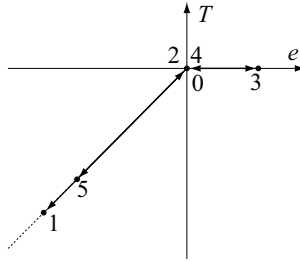
Figure 1. Stress-strain plot for a no-tension material in one dimension. A strain cycle is considered: $0 \to 1 \to 2$ (shortening cycle), $2 \to 3 \to 4$ (lengthening cycle), and $4 \to 5$ (further shortening). During shortening $T = Ee$ and $\lambda = 0$ (E being the Young's modulus), and during lengthening $T = 0$ and $\lambda = e$.

While in the one-dimensional case the existence of a strain energy density is assured, to obtain hyperelasticity in the two-dimensional case there is a price to pay: the assumption of normality must be made on the total latent strain λ (conditions $(2\text{-}6)_4$ and $(2\text{-}6)_5$). Such an assumption implies that on a discontinuity line Γ for the displacement, that is, the support of concentrated fractures, the jump of displacement must be orthogonal to Γ. Therefore sliding is forbidden on fracture lines.

It is shown in [Del Piero 1989] that for NENT materials the major symmetry of $\mathbb{A}$ is necessary and sufficient to get existence of an energy function. In the isotropic case (plane stress) the energy density φ is easily expressed in terms of the eigenvalues e_1 and e_2 ($e_1 \le e_2$) of e:

$$\varphi(e) = \begin{cases} 0 & \text{if } e_1 \ge 0, \\ \frac{1}{2} E e_1^2 & \text{if } e_1 < 0 \text{ and } e_2 \ge -\nu e_1, \\ \dfrac{E}{2(1-\nu^2)}(e_1^2 + e_2^2 + 2\nu e_1 e_2) & \text{if } e_1 < 0 \text{ and } e_2 < -\nu e_1, \end{cases} \qquad (2\text{-}13)$$

where E is the Young's modulus and ν the Poisson's ratio. Notice that the stress T, derived from φ by using (2-3), satisfies identically the no-tension restriction, that is, there is no need to impose it as a constraint. A representation of φ in the space of principal total strains is given in Figure 2.
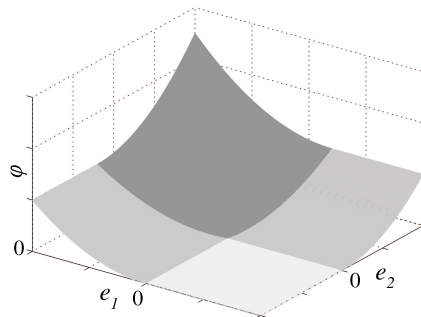

Figure 2. Strain energy density function for isotropic NENT material in two dimensions. In dark gray the parabolic sector corresponding to the biaxial compression is shown. In gray are the cylindrical regions of uniaxial compression, and in light gray the flat region of potential biaxial fractures.

For hyperelastic materials equilibrium states of the body can be sought as minimizers of the total potential energy (2-1):

$$\min_{\boldsymbol{u} \in \mathcal{K}} \mathcal{E}(\boldsymbol{u}), \qquad (2\text{-}14)$$

$\mathcal{K}$ being the set

$$\mathcal{K} = \{\boldsymbol{u} \in \mathcal{S}(\Omega) : \boldsymbol{u} = \bar{\boldsymbol{u}} \text{ on } \partial\Omega_N\} \qquad (2\text{-}15)$$

for $\mathcal{S}(\Omega)$ a convenient Banach space (see Appendix A).

2A5. *Numerical minimization strategy.* The numerical method we adopt to search for the minimum of the potential energy (2-1) is based on the direct minimization of such a functional through a descent method (steepest descent, conjugate gradient). The search is carried out in the subset of $\mathcal{K}$ defined by the C^0 displacement fields obtained by employing a standard finite element approximation based on a triangular finite element discretization Π_h of the domain Ω, where h is the mesh size. This kind of discretization excludes discontinuities in $\boldsymbol{u}$, that is, real cracks. The reason for considering such a simplification is twofold: Firstly, the authors believe that fractures in NENT material will appear smeared within the domain if the loads are not collapse loads in the sense specified in Appendix A. Secondly, in limit cases in which the loads approach the collapse limit the fracture strain may accumulate in narrow bands indicating the occurrence of real cracks in the limit.

The functional $\mathcal{E}$ is then approximated with the function $\mathfrak{E}(\{u_h\})$ of the nodal displacements $\{u_h\}$:

$$\mathfrak{E}(\{u_h\}) = -\sum_r L_r \boldsymbol{p}(\boldsymbol{x}_r) \cdot \boldsymbol{u}_r - \sum_m \boldsymbol{F}_m \cdot \boldsymbol{u}_m - \sum_n A_n \boldsymbol{b}(\boldsymbol{x}_n) \cdot \boldsymbol{u}_n + \sum_q A_q \varphi(\boldsymbol{x}_q), \qquad (2\text{-}16)$$

where $\boldsymbol{u}_r$ is the displacement at the midpoint $\boldsymbol{x}_r$ of the r-th edge of length L_r on $\partial\Omega_n$, $\boldsymbol{u}_m$ the displacement of the m-th mesh node where the concentrated force $\boldsymbol{F}_m$ is applied, $\boldsymbol{u}_n$ the displacement of the Gauss point $\boldsymbol{x}_n$ of the n-th mesh triangle with area A_n, and $\boldsymbol{x}_q$ the Gauss point of the q-th mesh triangle of area A_q where the strain energy density φ is evaluated for integration. In (2-16) all the displacements $\boldsymbol{u}_j$, as well as the strain energy density $\varphi(\boldsymbol{x}_q)$ in the q-th triangle, are clearly explicit functions of the nodal displacements $\{u_h\}$ via the linear shape functions of a standard triangular mesh.

The iterative procedure adopted to minimize the function (2-16) is based on a step-by-step minimization method. Let us indicate with $\{u_h\}_j$ the nodal displacements at the j-th minimization step. The force acting on the mesh nodes is given by the negative gradient of the energy $\boldsymbol{F}(\{u_h\}_j) = -\nabla\mathfrak{E}(\{u_h\}_j)$. The descent method implemented computes the velocity $\boldsymbol{p}_j$ employing the nodal forces at the current and previous step as

$$\boldsymbol{p}_j = \eta_j \boldsymbol{p}_{j-1} + \boldsymbol{F}(\{u_h\}_j), \qquad (2\text{-}17)$$

where the scalar η_j is

$$\eta_j = \max\left\{\frac{\boldsymbol{F}(\{u_h\}_j) \cdot \big(\boldsymbol{F}(\{u_h\}_j) - \boldsymbol{F}(\{u_h\}_{j-1})\big)}{\boldsymbol{F}(\{u_h\}_{j-1}) \cdot \boldsymbol{F}(\{u_h\}_{j-1})}, 0\right\}, \qquad (2\text{-}18)$$

in the Polak–Ribière version of the conjugate gradient method, and

$$\eta_j = \frac{\boldsymbol{F}(\{u_h\}_j) \cdot \boldsymbol{F}(\{u_h\}_j)}{\boldsymbol{F}(\{u_h\}_{j-1}) \cdot \boldsymbol{F}(\{u_h\}_{j-1})}, \qquad (2\text{-}19)$$

if the Fletcher–Reeves variant of the method is employed. (The Polak–Ribière method is usually adopted in the applications reported herein.)

If the nodes of the mesh are constrained, the velocity $\boldsymbol{p}_j$ is projected onto the tangent space of the constraints equation to obtain the compatible velocity $\boldsymbol{p}_j^*$. The velocity $\boldsymbol{p}_j^*$ gives the direction for the minimization motion while obeying all the constraints imposed on the nodes. The nodal displacement $\{u_h\}_j$ is computed as

$$\{u_h\}_j = \{u_h\}_{j-1} + \kappa_j \boldsymbol{p}_j^*, \tag{2-20}$$

where κ_j is the amplitude of the minimization step in the direction of $\boldsymbol{p}_j^*$ and is computed via line search method[1] to minimize the energy $\mathfrak{E}(\{u_h\})$ in the direction of the velocity $\boldsymbol{p}_j^*$. The iteration stops when a suitable norm of the energy gradient $\|\nabla\mathfrak{E}(\{u_h\}_j)\|$ becomes sufficiently small (see [Angelillo et al. 2008] for decrease conditions).

Descent methods appear very efficient in approximating the solutions of elastic problems with unilateral constraints on stress since the problem is reduced to the unconstrained minimization of a convex function. So far, there are no other computer programs of comparable simplicity for the stress analysis of no-tension materials. Numerical code for the approximation of the elastostatic problems of no-tension materials has been recently proposed in [Alfano et al. 2000; Lucchesi et al. 2008a], but such computer programs are still at a preliminary research stage.

The ability of descent methods to approximate the solution of boundary value problems for NENT materials is tested in this paper in two ways. The numerical solutions are compared first with some simple exact solutions, then with some experimental results. Finally the numerical solutions obtained with our code for more complex boundary value problems concerning masonry façades are presented.

2B. *The equilibrium problem for ML materials.* The crushing behavior of masonry is modeled as perfectly plastic. The initial-boundary value problem describing the quasistatic evolution of a no-tension elastoplastic body occupying a bounded domain Ω with boundary $\partial\Omega$ is then considered. Plastic behavior is described in terms of strain rates and the problem is not merely a boundary value one. The evolution is assumed to be quasistatic, that is, to occur so slowly that inertial and viscous effects may be ignored.

2B1. *The initial-boundary value problem in two dimensions.* Again we assume small strains and restrict ourselves to two-dimensional problems. The plastic behavior of the material is assumed to be represented within the classical framework of a convex elastic domain coupled with the normality law. The yield surface is assumed to be fixed in the stress space (no hardening or softening).

We consider given time dependent data such as fields $\boldsymbol{b}(\boldsymbol{x}, t)$ (body forces per unit volume), $\boldsymbol{p}(\boldsymbol{x}, t)$ (surface tractions per unit area), and $\bar{\boldsymbol{u}}(\boldsymbol{x}, t)$ (surface displacements):

$$\begin{aligned} \boldsymbol{b}: \quad &(\boldsymbol{x}, t) \in \Omega \times [0, \bar{t}) \rightarrow V^2, \\ \boldsymbol{p}: \quad &(\boldsymbol{x}, t) \in \partial\Omega_N \times [0, \bar{t}) \rightarrow V^2, \\ \bar{\boldsymbol{u}}: \quad &(\boldsymbol{x}, t) \in \partial\Omega_D \times [0, \bar{t}) \rightarrow V^2, \end{aligned} \tag{2-21}$$

with $[0, \bar{t})$ the time interval we consider and $\bar{t}$ the final instant of the simulation. Usually it is assumed that

$$\boldsymbol{b}(\boldsymbol{x}, 0) = \boldsymbol{0}, \quad \boldsymbol{p}(\boldsymbol{x}, 0) = \boldsymbol{0}, \quad \bar{\boldsymbol{u}}(\boldsymbol{x}, 0) = \boldsymbol{0}. \tag{2-22}$$

---

[1]The line search method calculates the energy for several values of the scale factor κ_j (doubling or halving each time) until the minimum energy is passed. The optimum scale is then calculated by quadratic interpolation.

Under the small strain hypothesis, the total deformation is again described by (2-2), and the additive decomposition of the total strain can be considered as

$$\boldsymbol{e} = \boldsymbol{\varepsilon}^e + \boldsymbol{\varepsilon}^p, \tag{2-23}$$

where $\boldsymbol{\varepsilon}^p$ is the plastic strain. Notice that now $\boldsymbol{\varepsilon}^e$ represents the total elastic deformation:

$$\boldsymbol{\varepsilon}^e = \boldsymbol{\varepsilon} + \boldsymbol{\lambda}, \tag{2-24}$$

the sum of

$$\boldsymbol{\varepsilon} = \mathbb{A}[\boldsymbol{T}], \tag{2-25}$$

where $\mathbb{A}$ is the compliance tensor, and

$$\boldsymbol{\lambda} \in \mathrm{P\,Sym}, \quad \boldsymbol{T} \cdot \boldsymbol{\lambda} = 0. \tag{2-26}$$

Assuming that the system is initially at rest in the natural state the initial conditions are

$$\boldsymbol{u}(\boldsymbol{x}, 0) = \boldsymbol{0} \quad \text{and} \quad \boldsymbol{T}(\boldsymbol{x}, 0) = \boldsymbol{0}. \tag{2-27}$$

The constitutive equations are defined on introducing the free energy $\varphi(\boldsymbol{\varepsilon}^e)$ and on specifying the flow law governing the evolution of the plastic strain. In particular $\varphi(\boldsymbol{\varepsilon}^e)$ is taken of the form (2-13):

$$\varphi(\boldsymbol{\varepsilon}^e) = \begin{cases} 0 & \text{if } \varepsilon_1^e \geq 0, \\ \frac{1}{2} E (\varepsilon_1^e)^2 & \text{if } \varepsilon_1^e < 0 \text{ and } \varepsilon_2^e \geq -\nu\varepsilon_1^e, \\ \dfrac{E}{2(1-\nu^2)} \big((\varepsilon_1^e)^2 + (\varepsilon_2^e)^2 + 2\nu\varepsilon_1^e\varepsilon_2^e \big) & \text{if } \varepsilon_1^e < 0 \text{ and } \varepsilon_2^e < -\nu\varepsilon_1^e, \end{cases} \tag{2-28}$$

ε_1^e and ε_2^e being the eigenvalues of $\boldsymbol{\varepsilon}^e$. The stress $\boldsymbol{T}$ is then assumed to be given by

$$\boldsymbol{T} = \frac{\partial \varphi(\boldsymbol{\varepsilon}^e)}{\partial \boldsymbol{\varepsilon}^e}. \tag{2-29}$$

We further assume that the stress cannot be arbitrarily large but is confined to belong to a bounded convex set K of Sym containing the origin. The interior of $K \cap \mathrm{N\,Sym}$ is the elastic region while its boundary is the yield surface. Notice that $K \cap \mathrm{N\,Sym}$ is convex but need not to be smooth. The boundary of K may be represented by the level set of a function f, called the crushing function, so that

$$K = \{\boldsymbol{T} \in \mathrm{Sym} : f(\boldsymbol{T}) \leq 0\}. \tag{2-30}$$

For the time rate $\dot{\boldsymbol{\varepsilon}}^p$ of the plastic strain we consider the associative flow law

$$(\boldsymbol{T}' - \boldsymbol{T}) \cdot \dot{\boldsymbol{\varepsilon}}^p \leq 0 \ \text{ for } \boldsymbol{T}' \in K. \tag{2-31}$$

For simplicity we consider

$$f(\boldsymbol{T}) = \varphi\big(\boldsymbol{\varepsilon}^e(\boldsymbol{T})\big) - \frac{\sigma_0^2}{2E}, \tag{2-32}$$

where $\varphi\big(\boldsymbol{\varepsilon}^e(\boldsymbol{T})\big) = \varphi(\mathbb{A}[\boldsymbol{T}] + \boldsymbol{\lambda}) = \varphi(\mathbb{A}[\boldsymbol{T}])$ is the strain energy density of the NENT material, expressed here as a function of the stress $\boldsymbol{T}$, and σ_0 is the crushing stress in axial compression, that is, the boundary of K is a level set of the free energy of the NENT material. Figure 3 depicts a section of the elastic domain on the plane $T_{12} = 0$.
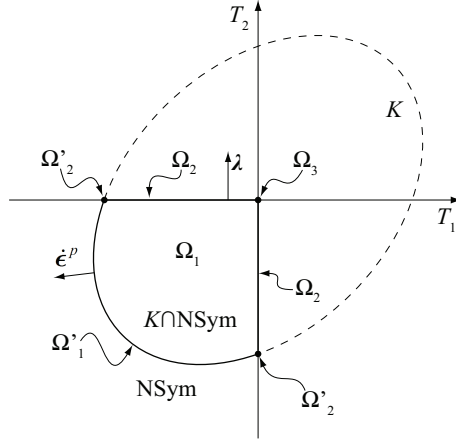
Figure 3. Elastic domain in the plane $T_{12} = 0$. The regions Ω_i' are the plastic duals of the regions Ω_i defined in (2-10), i.e., in Ω_1' the material is yielding in biaxial compression while in Ω_2' it is yielding in uniaxial compression. A point $x \in \Omega$ lies in Ω_1 if and only if $T(x) \in (\mathrm{N\,Sym} \cap K)$, and it lies in the union $\Omega_1' \cup \Omega_2 \cup \Omega_2' \cup \Omega_3$ if and only if $T(x) \in \partial(\mathrm{N\,Sym} \cap K)$.

2B2. *Energy formulation, internal variables.* We choose to describe the problem in terms of the total strain and of the recorded history of mechanical behavior, by introducing as an internal variable the total plastic strain $\boldsymbol{\varepsilon}^p$. If we consider that the form of $\varphi(\boldsymbol{e}, \boldsymbol{\varepsilon}^p)$ is prescribed and that $\boldsymbol{T} = \partial\varphi/\partial\boldsymbol{\varepsilon}^e$, the instantaneous values of $\boldsymbol{T}$ are known if $\boldsymbol{e}$ is given and the entire process of plastic strain is known. Obviously $\boldsymbol{\varepsilon}^p(t) = \int_0^t \dot{\boldsymbol{\varepsilon}}^p(\tau)d\tau$ and $\dot{\boldsymbol{\varepsilon}}^p$ is described by the flow rule (2-31). In the one-dimensional case the stress-deformation behavior, the admissible region in the (e, ε^p) space and the form of φ, represented by a three-dimensionalgraph in the space $(e, \varepsilon^p, \varphi)$, are depicted in Figure 4, where a typical loading path
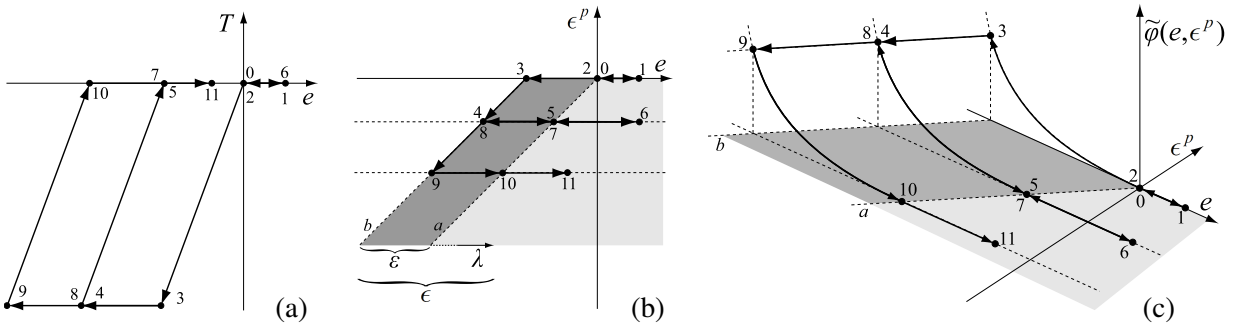
Figure 4. Example of loading-unloading paths of an ML material in one dimension depicted in (a) the (e, T) plane, (b) the (e, ε^p) plane, and (c) the $(e, \varepsilon^p, \varphi)$ space: $0 \to 1 \to 2$ (lengthening cycle), $2 \to 3 \to 4 \to 5$ (shortening cycle in elastoplastic regime), $5 \to 6 \to 7$ (lengthening cycle), $7 \to 8 \to 9 \to 10$ (shortening cycle), and $10 \to 11$ (further lengthening). The material is fractured in the light gray area and compressed in the dark gray area, while plastic strain increases during the compressions $3 \to 4$ and $8 \to 9$.

is reported. Notice that, based on the ML model, fracture strains are reversible and are perfectly recoiled upon load inversion. Crushing strains, by contrast, cannot be healed and, being totally irreversible, can either stay or grow. In other words, smeared fractures cannot cancel crushing strains; the two mechanisms are completely independent.

2B3. *Numerical minimization strategy.* The time interval $[0, \bar{t})$ is discretized into k subintervals by means of the instants $0 = t_0 \leq \cdots \leq t_i \cdots \leq t_k = \bar{t}$. The idea is to solve, at each time step t_i, the minimum problem of a suitably defined, updated functional characteristic of an evolving no-tension material with a nonlinear elastic behavior in compression, to approximate the solution path $\zeta(t) = \big(\boldsymbol{u}(t), \boldsymbol{\varepsilon}^p(t)\big)$ which solves the initial-boundary value problem defined above.

To model perfect plasticity in compression, we assume a linearly-growing extension of the strain energy function (2-13) above the yield surface defined by (2-32). Namely, at time step t_i, the functional form implemented in the finite element code is

$$
\tilde{\varphi}_i(\boldsymbol{\varepsilon}_i^e) = \begin{cases}
0 & \text{if } (\varepsilon_i^e)_1 \geq 0, \ (\varepsilon_i^e)_2 \geq 0, \\[2mm]
\frac{1}{2} E (\varepsilon_i^e)_1^2 & \text{if } (\varepsilon_i^e)_1 < 0, \ (\varepsilon_i^e)_2 \geq -\nu(\varepsilon_i^e)_1, \ f(\boldsymbol{\varepsilon}_i^e) \leq 0, \\[2mm]
\alpha \sqrt{\frac{1}{2} E (\varepsilon_i^e)_1^2} + \beta & \text{if } (\varepsilon_i^e)_1 < 0, \ (\varepsilon_i^e)_2 \geq -\nu(\varepsilon_i^e)_1, \ f(\boldsymbol{\varepsilon}_i^e) > 0, \\[2mm]
\frac{E}{2(1-\nu)}\big((\varepsilon_i^e)_1^2 + (\varepsilon_i^e)_2^2 + 2\nu(\varepsilon_i^e)_1(\varepsilon_i^e)_2\big) & \text{if } (\varepsilon_i^e)_1 < 0, \ (\varepsilon_i^e)_2 < -\nu(\varepsilon_i^e)_1, \ f(\boldsymbol{\varepsilon}_i^e) \leq 0, \\[2mm]
\alpha \sqrt{\frac{E}{2(1-\nu^2)}\big((\varepsilon_i^e)_1^2 + (\varepsilon_i^e)_2^2 + 2\nu(\varepsilon_i^e)_1(\varepsilon_i^e)_2\big)} + \beta & \text{if } (\varepsilon_i^e)_1 < 0, \ (\varepsilon_i^e)_2 < -\nu(\varepsilon_i^e)_1, \ f(\boldsymbol{\varepsilon}_i^e) > 0,
\end{cases}
$$

$$(2\text{-}33)$$

where the elastic strain at time t_i is given by the difference between the total strain $\boldsymbol{e}_i$ at the same time step and the plastic strain inherited from the previous solution step $\boldsymbol{\varepsilon}_{i-1}^p$, i.e., $\boldsymbol{\varepsilon}_i^e = \boldsymbol{e}_i - \boldsymbol{\varepsilon}_{i-1}^p$, and $(\varepsilon_i^e)_j$ ($j = 1, 2$) are the principal values of $\boldsymbol{\varepsilon}_i^e$. The constants $\alpha = \sqrt{2/E}\sigma_0$ and $\beta = -\sigma_0^2/(2E)$ are introduced to preserve the C^1 regularity of $\tilde{\varphi}_i$. A representation of $\tilde{\varphi}_i$ in the space of principal elastic strains is given in Figure 5. The numerical method finds the minimum of the total potential energy defined at time t_i as

$$
\mathscr{E}_i(\boldsymbol{u}_i) = -\int_{\partial\Omega_N^i} \boldsymbol{p}_i \cdot \boldsymbol{u}_i \, ds - \int_\Omega \boldsymbol{b}_i \cdot \boldsymbol{u}_i \, da + \int_\Omega \tilde{\varphi}_i\big(\boldsymbol{e}_i(\boldsymbol{u}_i)\big) \, da, \tag{2-34}
$$

via finite element discretization of the domain Ω and descent minimization. The solution at the previous load step is used as the initial condition for the minimization of the function

$$
\mathfrak{E}_i(\{u_h\}_i) = -\sum_r L_r \boldsymbol{p}_i(\boldsymbol{x}_r) \cdot \boldsymbol{u}_r - \sum_m \boldsymbol{F}_m \cdot \boldsymbol{u}_m - \sum_n A_n \boldsymbol{b}_i(\boldsymbol{x}_n) \cdot \boldsymbol{u}_n + \sum_q A_q \tilde{\varphi}_i(\boldsymbol{x}_q), \tag{2-35}
$$

representing the finite element approximation of the total potential energy (2-34) as in the case of (2-16) for the NENT material. The minimization is performed via the descent method described in Section 2A5.

A plastic strain update is then performed at each Gauss point: Equation (2-32) defines a surface whose position vector is $\boldsymbol{s}$, of coordinates $\{s_j\}$, in the space of principal elastic strains $\boldsymbol{\varepsilon}_i^e$. It is useful to give a parametric description $\boldsymbol{s}(\boldsymbol{\gamma})$ of the yielding surface in the space of principal elastic strain, with $\boldsymbol{\gamma}$ being a suitable set of parameters. The return mapping algorithm, according to the principle of minimum
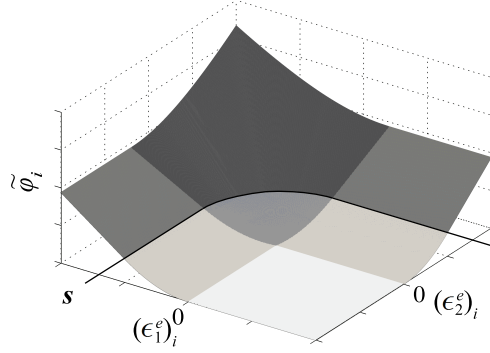
Figure 5. Strain energy density function for an isotropic ML material in two dimensions. It is evident here that, above the yielding curve s, the energy consists of an extension of the energy φ, depicted in Figure 2, characterized by a linear growth.

dissipation imposed by the assumption of associated plasticity [Ortiz and Simo 1986], consists in finding the set of parameters $\boldsymbol{\gamma}^0$ of minimum distance, in the energy norm, of the current elastic strain $\boldsymbol{\varepsilon}_i^e$ from the surface $\boldsymbol{s}(\boldsymbol{\gamma})$:

$$\min_{\boldsymbol{\gamma}} \varphi\big(\boldsymbol{s}(\boldsymbol{\gamma}) - \boldsymbol{\varepsilon}_i^e\big). \tag{2-36}$$

In the two-dimensional case considered here, the yielding surface is merely a curve in the plane of the principal elastic strains $(\varepsilon_i^e)_j$ ($j = 1, 2$), as depicted in Figure 5, and can be described by a single parameter γ. The minimum problem (2-36) can be easily formulated as

$$\frac{d}{d\gamma}\varphi\big(\boldsymbol{s}(\gamma) - \boldsymbol{\varepsilon}_i^e\big) = 0. \tag{2-37}$$

Equation (2-37) is solved for γ, at each Gauss point, via the Newton–Raphson method.

The tensor of plastic strain rate $\dot{\boldsymbol{\varepsilon}}^p$ at time t_i is coaxial to the elastic strain tensor $\boldsymbol{\varepsilon}_i^e$, therefore the principal components $(\Delta\varepsilon_i^p)_j$ (with $j = 1, 2$) of the plastic strain increment $\Delta\boldsymbol{\varepsilon}_i^p$ (i.e., the discrete version of $\dot{\boldsymbol{\varepsilon}}^p$) are simply computed as

$$(\Delta\varepsilon_i^p)_j = (\varepsilon_i^e)_j - s_j(\gamma^0). \tag{2-38}$$

Once the plastic strain has been updated in the global reference frame, i.e., $\boldsymbol{\varepsilon}_i^p = \boldsymbol{\varepsilon}_{i-1}^p + \Delta\boldsymbol{\varepsilon}_i^p$ (a backward Euler finite difference scheme), the energy density dissipation at the given Gauss point, at time step i, can be computed as

$$\mathcal{D}_i = \tilde{\varphi}_i(\boldsymbol{e}_i, \boldsymbol{\varepsilon}_{i-1}^p) - \tilde{\varphi}_i(\boldsymbol{e}_i, \boldsymbol{\varepsilon}_i^p) = \tilde{\varphi}_i(\boldsymbol{e}_i, \boldsymbol{\varepsilon}_{i-1}^p) - \tfrac{1}{2}\boldsymbol{T}_i\mathbb{A}[\boldsymbol{T}_i], \tag{2-39}$$

where it is clear from the first expression that the plastic strain increments dissipate energy. The stress tensor $\boldsymbol{T}_i$ in the second expression is computed via (2-29).

3. Comparing numerical with analytical/semianalytical solutions for NENT materials

3A. *Flexure of a NENT panel.* The first problem we consider is the flexure of a rectangular strip. The geometry and the boundary conditions are depicted in Figure 6 to which we refer for notation.

A simple solution of the problem exists if the material is isotropic and $v = 0$. The displacement field $\boldsymbol{u} = u\hat{\boldsymbol{i}} + v\hat{\boldsymbol{j}}$, $\hat{\boldsymbol{i}}$ and $\hat{\boldsymbol{j}}$ being the unit vectors in the x and y directions respectively, with

$$u = \frac{\Phi}{H}(H - 2x)y, \quad v = \frac{\Phi}{H}x(x - H), \tag{3-1}$$

solves all the field and boundary equations for an isotropic NENT material with $v = 0$. Indeed the corresponding total strain is

$$\boldsymbol{e} = -\frac{2\Phi}{H}y\hat{\boldsymbol{i}} \otimes \hat{\boldsymbol{i}}, \tag{3-2}$$

which is easily decomposed into the elastic and fracture parts:

$$\boldsymbol{\varepsilon} = \begin{cases} \boldsymbol{e} & \text{if } y > 0, \\ \boldsymbol{0} & \text{if } y \le 0, \end{cases} \qquad \boldsymbol{\lambda} = \begin{cases} \boldsymbol{0} & \text{if } y > 0, \\ \boldsymbol{e} & \text{if } y \le 0. \end{cases} \tag{3-3}$$

The corresponding stress field is

$$\boldsymbol{T} = \begin{cases} -E\dfrac{2\Phi}{H}y\hat{\boldsymbol{i}} \otimes \hat{\boldsymbol{i}} & \text{if } y > 0, \\ \boldsymbol{0} & \text{if } y \le 0. \end{cases} \tag{3-4}$$

This stress field is obviously balanced with the prescribed loads $\boldsymbol{b} = \boldsymbol{0}$ at the interior and with the surface tractions $\boldsymbol{p} = \boldsymbol{0}$ given at the boundary $|x| = B/2$. Based on this solution for the stress the domain Ω is split into two zones of type Ω_2, Ω_3 as depicted in Figure 6. This example can give some evidence of the nonuniqueness of the solution and particularly the possibility of different fracture fields under the same boundary conditions.

Indeed another solution to the same problem is defined by the displacement field $\boldsymbol{u} = u\hat{\boldsymbol{i}} + v\hat{\boldsymbol{j}}$ with

$$u = \begin{cases} \Phi(y/H)(H - 2x) & \text{if } y > 0, \\ \Phi y & \text{if } y < 0 \text{ and } x < H/2, \\ -\Phi y & \text{if } y < 0 \text{ and } x > H/2, \end{cases} \tag{3-5}$$
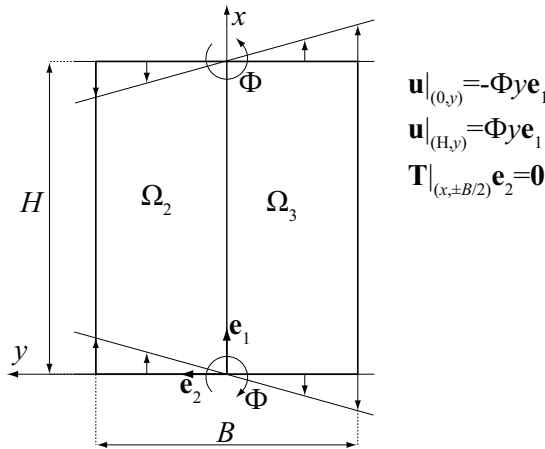
Figure 6. Flexure of a NENT panel: coordinates, nomenclature, boundary conditions, and partition of the domain.

and

$$v = \begin{cases} \Phi(x/H)(x - H) & \text{if } y > 0, \\ -\Phi x & \text{if } y < 0 \text{ and } x < H/2, \\ \Phi(x - H) & \text{if } y < 0 \text{ and } x > H/2. \end{cases} \tag{3-6}$$

The corresponding total strain is composed of absolutely continuous and singular parts: $e = e^a + e^s$ with

$$e^a = \begin{cases} -2\Phi(y/H)\hat{\imath} \otimes \hat{\imath} & \text{if } y > 0, \\ 0 & \text{if } y \le 0, \end{cases} \tag{3-7}$$

and

$$e^s = \begin{cases} (\Phi/H)x^2\delta(y)\hat{\jmath} \otimes \hat{\jmath} & \text{if } x \le H/2, \\ (\Phi/H)(x - H)^2\delta(y)\hat{\jmath} \otimes \hat{\jmath} & \text{if } x > H/2, \\ -2\Phi y\delta(x - H/2)\hat{\imath} \otimes \hat{\imath} & \text{if } y \le 0, \\ 0 & \text{otherwise.} \end{cases} \tag{3-8}$$

Here $\delta(\xi)$ denotes the line Dirac delta at $\xi = 0$. The total strain is decomposed in its elastic and fracture parts as follows:

$$\boldsymbol{\lambda} = e^s, \quad \boldsymbol{\varepsilon} = e^a. \tag{3-9}$$

Therefore the stress T is the same as that of the first solution and determines the same partition of the domain Ω as described in Figure 6.

The fracture strain is singular and corresponds to the cracks exhibited by the deformed configuration depicted in Figure 7, left. Graphs of the λ_{11} and λ_{22} components of $\boldsymbol{\lambda}$ are reported in Figure 7, middle.

In the absence of any energy price to pay to open up fractures the two solutions reported are perfectly equivalent and the body can choose any of the two. It could be of some interest to look at the result of a flexure test performed on an ML material (a composite of lime, gypsum, and pozzolana with a ratio between tensile and compressive strength of $1/30$) shown in Figure 7, right.

In the numerical simulations we assumed $\nu = 0$, $E = 660\,\text{MPa}$, $\Phi = 0.001$, $H = B = 2\,\text{m}$, and thickness equal to 0.5 m. Figure 8, left, is a contour plot of the maximum eigenvalue of the fracture strain. Fractures are nonzero in the region indicated by Ω_3 in Figure 6, and their distribution suggests that the numerical solution is close to the rigid-block scheme of Figure 8, right, which can be an energetically-equivalent alternative to the two solutions introduced above.
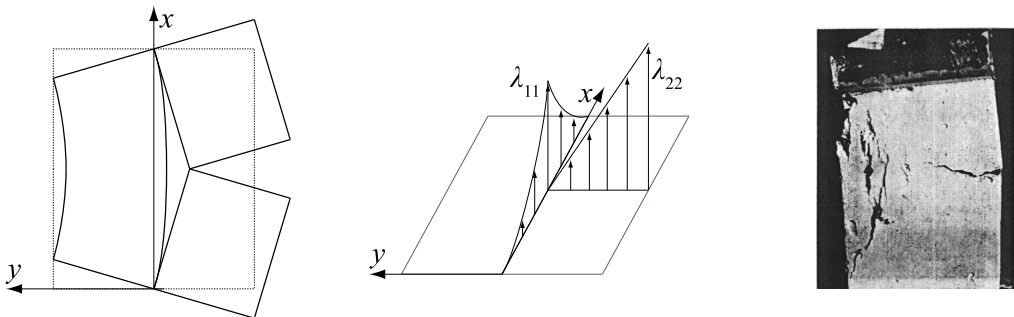
Figure 7. Flexure of a NENT panel. Left: deformed configuration corresponding to the solution described in (3-5)–(3-9). Middle: plot of the singular part of the strain described by (3-8)$_2$. Right: flexure test on a masonry panel (courtesy of G. Castellano).
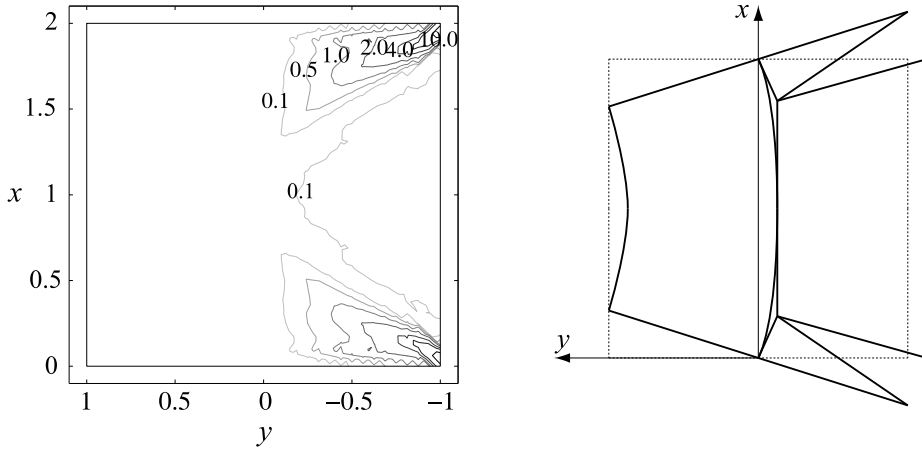
Figure 8. Flexure of a NENT panel. Left: maximum fracture strain $[10^{-3}]$. Right: rigid-block kinematic close to the numerical solution.

We performed a numerical convergence study on the stress for the flexure problem of a NENT panel by considering a sequence of discretizations of decreasing mesh size h. The result is reported in Figure 9. The top row of Figure 10 shows the different discretizations of the domain Ω employed in the convergence analysis. The related level plots of the maximum stress compared to the exact solution described by (3-4) are depicted in the bottom row of Figure 10, to show graphically the rate of convergence.

In Figure 9 we plot the correlation between the approximation error for the stress

$$e_h = \frac{\|\boldsymbol{T}_h - \boldsymbol{T}_0\|_{L^2}}{\|\boldsymbol{T}_h\|_{L^2}} \tag{3-10}$$

and the dimensionless mesh size h/D, where $D = \sqrt{H^2 + B^2}$ is the diameter of Ω, $\boldsymbol{T}_h$ is the stress field computed with a mesh of size h and $\boldsymbol{T}_0$ is the exact solution. A linear convergence of the method is obtained.
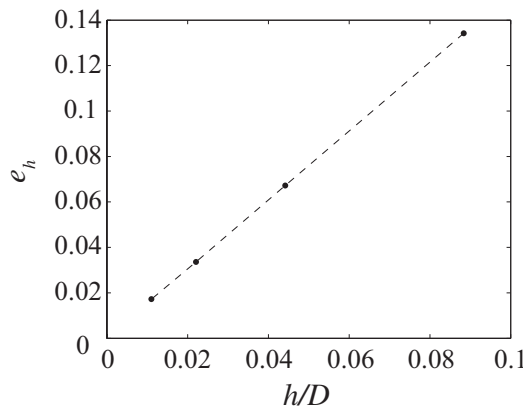
Figure 9. Flexure of a NENT panel: convergence diagram.
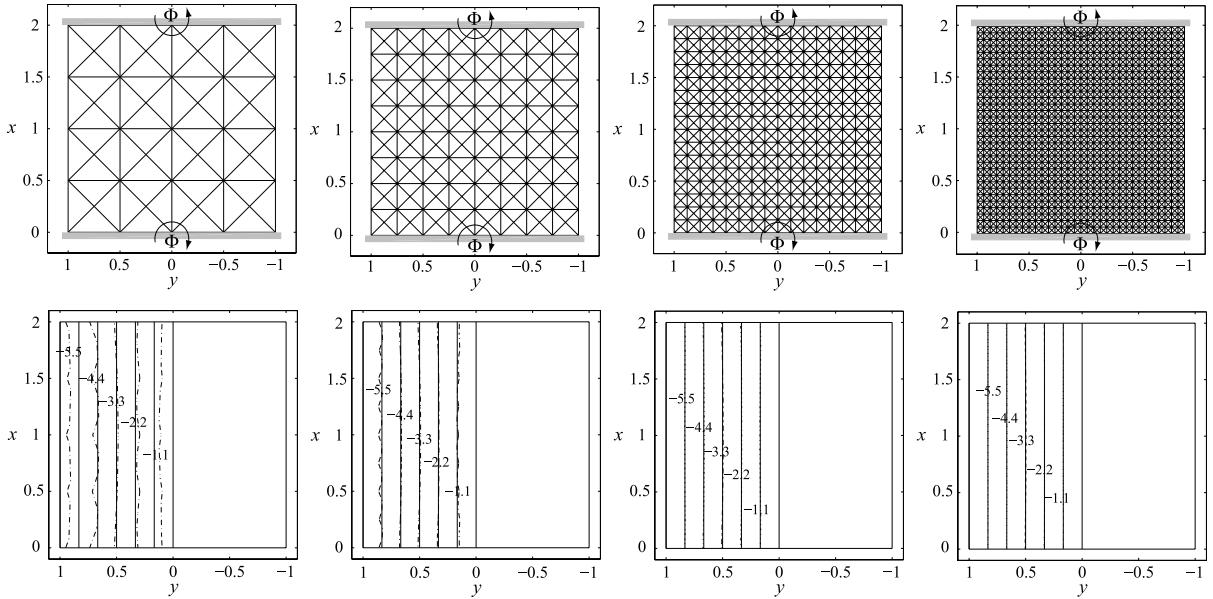
Figure 10. Flexure of a NENT panel. Top: meshes employed for the simulations in the convergence analysis. Bottom: progressive convergence of the computed maximum stress contour plot (dash-dotted curves) [10^5 Pa] to the exact solution (solid curves).

3B. *Shear of a NENT panel.* The simple rectangular panel depicted in Figure 11 subject to a given relative horizontal translation of the bases (of value $2U$) and zero traction condition on the lateral sides is considered. The material parameters and the geometry are the same adopted in the previous section. The value $U = 1$ mm is considered.

In Figures 11 and 12 the numerical solution is compared to a semianalytical solution obtained by minimizing the complementary energy $\mathscr{E}_c$ (see Appendix B), restricting the search to uniaxial stress
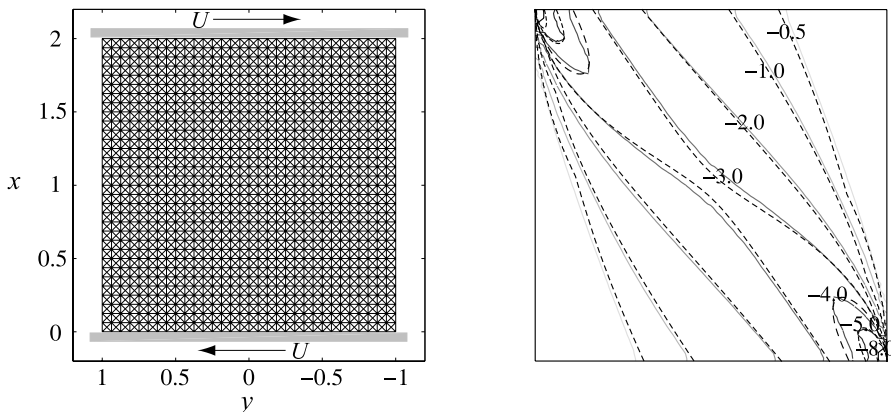
Figure 11. Shear of a NENT panel. Left: mesh and boundary conditions. Right: comparison of the maximum compressive stress [10^5 Pa] obtained via finite element solution (solid curves) with the semianalytical method of [Fortunato 2010] (dashed curves).
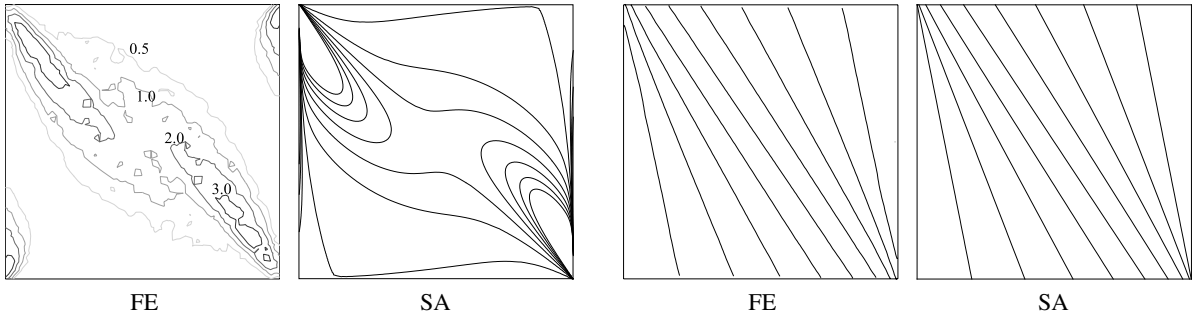
Figure 12. Shear of a NENT panel: maximum principal value of the fracture strain $[10^{-3}]$ (left two panes) and isostatic curves (right two panes), computed via finite elements (FE) and via the semianalytical approach (SA).

states, that is, assuming that $\Omega = \Omega_2 \cup \Omega_3$. The general case of arbitrary prescribed relative displacements between the two bases is considered and solved in [Fortunato 2010]. To make the present paper self contained we present in Appendix B the derivation of this semianalytical solution in the special case considered here. The distribution of the maximum compressive stress, the fracture strain, and the form of the isostatic lines computed numerically are in good agreement with the results of the semianalytical method of [Fortunato 2010], as summarized in Figures 11 and 12.

4. Comparing numerical solutions with analytical solutions and experiments for ML materials

4A. *Flexure of an ML panel.* The numerical experiment performed in Section 3A for a NENT panel is repeated here for an ML panel assuming $\Phi = 0.006$ and the maximum compressive strength $\sigma_0 = 19.8 \, \text{MPa}$. The value of $\Phi = 2\sigma_0 H / BE$ is selected in such a way that the strip $y > B/4$ is forced into the yielding regime. The exact stress solution is

$$\boldsymbol{T}_0 = \begin{cases} -\sigma_0 \hat{\boldsymbol{\imath}} \otimes \hat{\boldsymbol{\imath}} & \text{if } y \geq B/4, \\ -4\sigma_0 (y/B) \hat{\boldsymbol{\imath}} \otimes \hat{\boldsymbol{\imath}} & \text{if } 0 < y < B/4, \\ \boldsymbol{0} & \text{if } y \leq 0. \end{cases} \tag{4-1}$$

Again a sequence of discretizations of decreasing mesh size is considered. Figure 13a shows the computed isostatic curves. For the finest mesh they are very close to being vertical lines as expected. In Figure 13b we compare the level plot of the computed maximum compressive stress relative to the finest mesh (the solid lines) with the exact solution given by (4-1) (the dash-dotted lines). The solution shows good accuracy. The maximum fracture strain is reported in Figure 13c, and it can be noticed that the fracture distribution in the strip $y < 0$ (region Ω_3 in Figure 6) is similar to the one observed in the NENT material (see Figure 8a). The distribution of fracture strain in the Ω_2 region resembles closely the vertical fractures that appear in the experiment shown in Figure 13d. We point out here that, in this problem, the distribution of plastic strains is not unique since they only need to satisfy the integral relation

$$\int_0^H \lambda_{11}(x, y) \, dx = -\frac{2\Phi}{H} y + \frac{\sigma_0}{E} \quad \text{for } y \geq \frac{B}{4}. \tag{4-2}$$

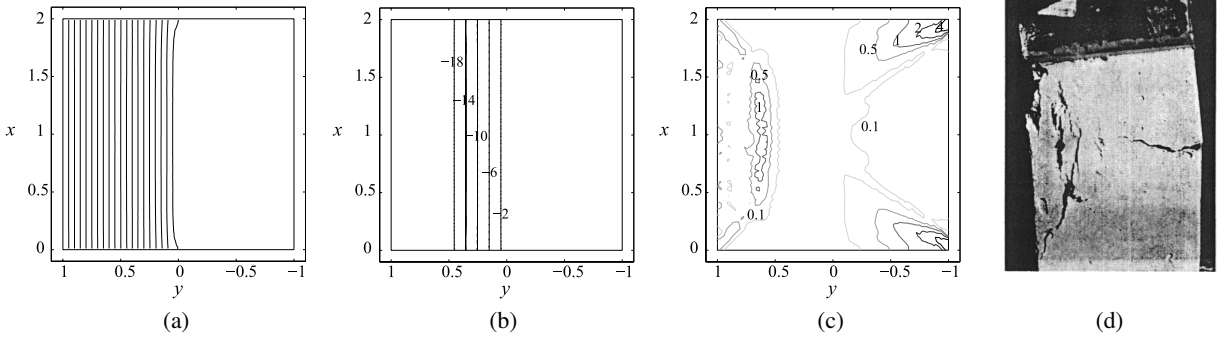(a)   (b)   (c)   (d)

Figure 13. Flexure of an ML panel: (a) isostatic curves, (b) contour plot of the computed maximum compression (the dash-dotted curves) compared to the exact solution [10^5 Pa], (c) contour plot of the maximum principal value of the fracture strain [10^{-3}] compared to (d) flexure test on a masonry panel (courtesy of G. Castellano).
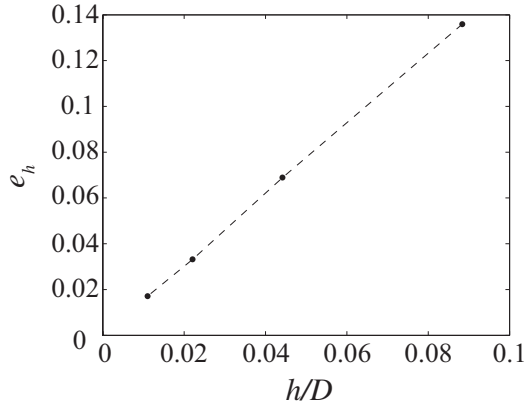

Figure 14. Flexure of an ML panel: convergence diagram.

Figure 14 shows the convergence diagram for the problem of flexure of an ML panel. The definitions of the normalized mesh size h/D and of the error e_h are the same introduced in Section 3A and the method converges again linearly to the exact solution given by (4-1).

4B. *Shear of an ML panel.* The value of the displacement at the boundary U considered in Section 3B is small enough to confine yielding in the material close to the corners of an ML panel that behaves essentially as a NENT panel. In this section we follow the evolution of the shear problem as the value of U increases and the crushing of the material progresses.

In Figure 15 we report three stages of the evolving solution. As the boundary displacement increases, a diagonal band, uniaxially and uniformly compressed at the limit stress $\sigma_0 = 1.98$ MPa, forms progressively and the isostatic lines become parallel.

The contour plots in Figure 16 show the maximum fracture strain, which concentrates on two subdiagonal lines, and the maximum plastic strain, which concentrates near the constrained boundary. The concentration of the plastic strain is expected, due to the perfect plasticity of the material.
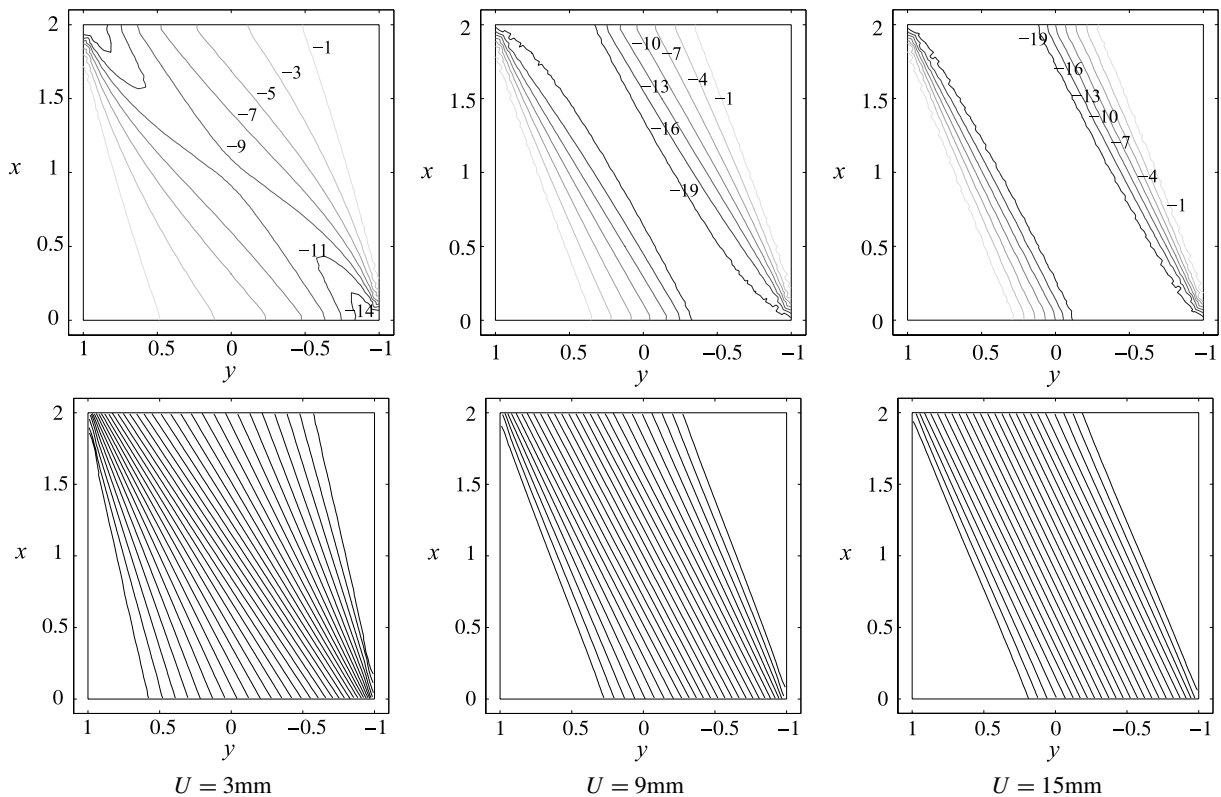
Figure 15. Shear of an ML panel: evolution as boundary displacement increases ($U = 3$ mm, 9 mm, 15 mm). Top: minimum principal stress [10^5 Pa]. Bottom: isostatic lines.
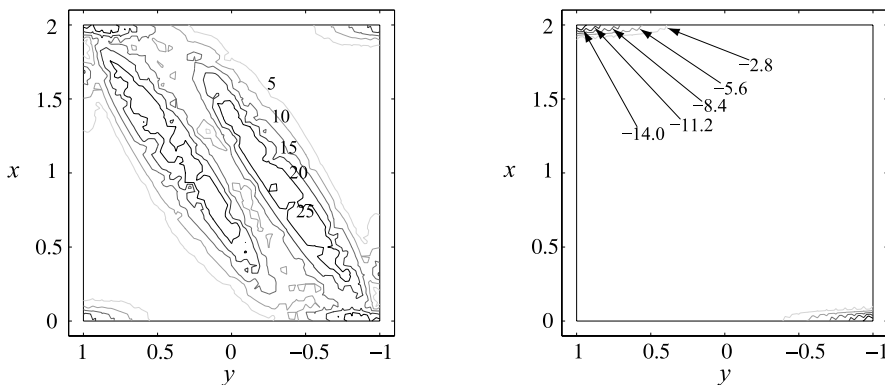
Figure 16. Shear of an ML panel: contour plots of the maximum principal value of the fracture strain [10^{-3}] (left) and the plastic strain [10^{-2}] (right).

Figure 17, left, represents the behavior of the energy as a function of the discrete increment of the boundary displacement U: at each time step i in the process the energy level denoted by • represents the computed solution, the point denoted by ∘ is the energy level corresponding to the increment of the
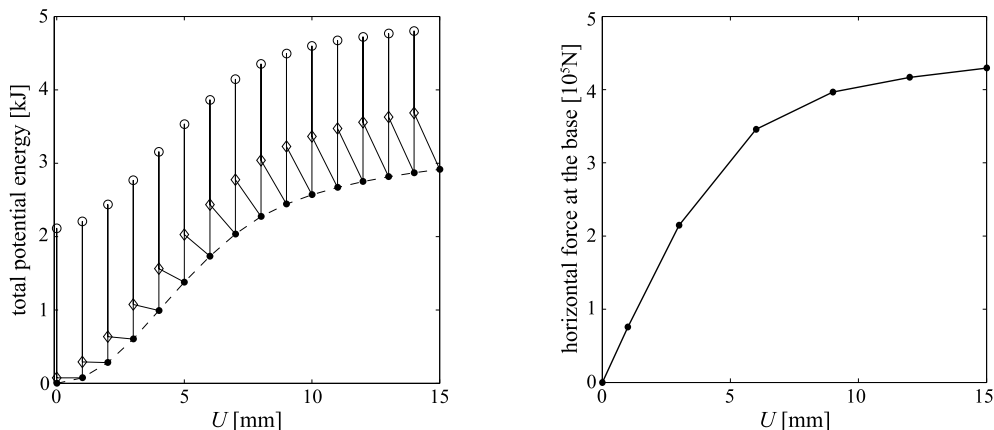
Figure 17. Shear of an ML panel. Left: energy history in the computational process. Right: evolution of the computed reaction at the base.

boundary condition at the step $i + 1$ and the point denoted by $\diamond$ corresponds to the energy level after the convergence of the minimization procedure. Therefore the branch $\bullet_i \to \circ_i$ represents the effect of updating the load from the value at time i to the one at time $i + 1$, $\circ_i \to \diamond_i$ the effect of the numerical minimization of $\mathscr{E}_{i+1}$, and $\diamond_i \to \bullet_{i+1}$ the effect of the numerical update of the plastic strain that gives the solution at time $i + 1$. The energy drop in the branch $\diamond_i \to \bullet_{i+1}$ represents energy dissipation that can be computed integrating over the domain Ω, with the dissipation density $\mathscr{D}_i$ given by (2-39). The dashed line is the envelope of the solution points representing the numerical approximation of the time history of the total potential energy. In Figure 17, right, the evolution of the horizontal component of the computed reaction at the base (the horizontal force) as the displacement U_i increases is depicted. The shear force plateaus as expected for a structure close to collapse.

4C. *Validation against experimental tests.* In this section we validate the ML material model against independent sets of experimental results from [Benedetti and Steli 2008] and [Eucentre 2008], performed on different types of masonry. Figure 18 depicts the clamped-clamped load scheme used in the simulations. It reproduces the setup used in both the experimental sets: a masonry panel of width B, height H, and thickness D is clamped to the ground at the bottom and to a steel beam at the top (the gray strip in Figure 18). A uniform load is distributed at the top part of the steel beam and the horizontal load is applied in incremental steps by imposing the horizontal displacement U of the left extreme of the steel beam. Table 1 on page 604 lists the geometrical and material parameters for the experiments simulated. Neither [Benedetti and Steli 2008] and [Eucentre 2008] report measurements of the Poisson's ratio, and because of that we take $\nu = 0$ in the simulations. Nevertheless, parametric studies, not reported here, show that the simulated force-displacement curves manifest very low sensitivity to the Poisson's ratio.

The graphs in the top row of Figure 19 compare the numerical simulations and the experimental results for specimens 1A-08 and 2C-03 of [Benedetti and Steli 2008], made of crushed stone and injected crushed stone masonry. The model reproduces quantitatively the substantial features of the measured force-displacement curves, with a slight overestimation of the force for higher levels of the horizontal displacement U.
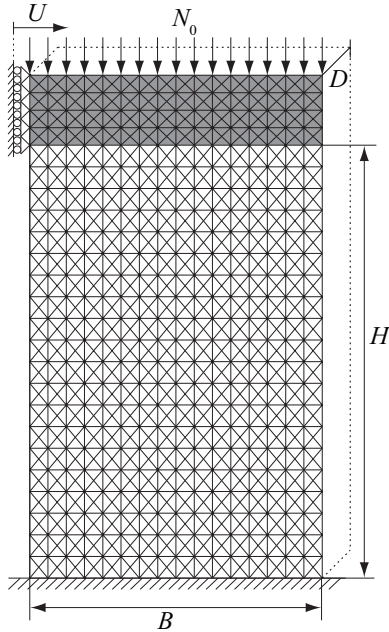
Figure 18. Load scheme of the simulation reproducing the experimental setup used in [Benedetti and Steli 2008; Eucentre 2008].
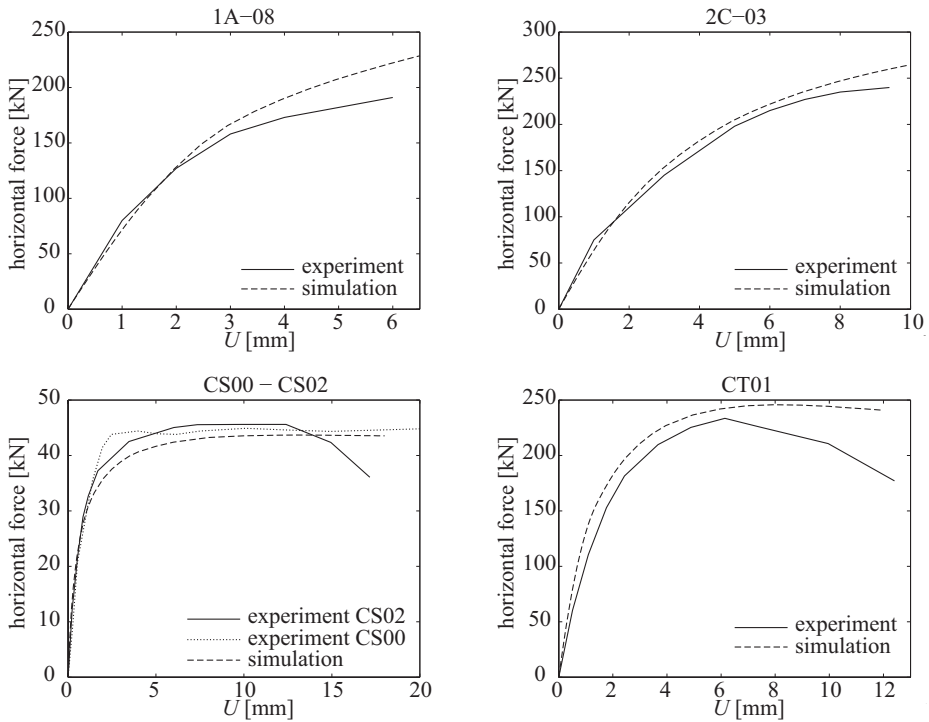

Figure 19. Comparison of numerical simulations with experimental results from [Benedetti and Steli 2008] (top row) and [Eucentre 2008] (bottom row).

Experiment	Material	B [m]	H [m]	D [m]	E [MPa]	ν	σ_0 [MPa]	N_0 [MPa]
1A-08	Crushed stone	1.25	1.85	0.50	1290	0.0	3.69	0.57
2C-03	Injected crushed stone	1.25	1.82	0.50	1118	0.0	6.00	0.55
CS00-CS02	Stone	1.25	2.50	0.32	3000	0.0	3.30	0.20
CT01	Stone	2.50	2.50	0.32	3000	0.0	3.30	0.50

Table 1. Structural and material parameters used in the simulations of the experimental tests. The load scheme is reported in Figure 18. Experiments 1A-08 and 2C-03 [Benedetti and Steli 2008], and experiments CS00-CS02 and CT01 [Eucentre 2008].

The graphs in the bottom row of Figure 19 report the comparison between experimental data and numerical simulations for specimens CS00, CS02, and CT01 in [Eucentre 2008], all made of stone masonry. Specimen CS00 differs from the other two because the mortar has been reinforced with 20% sand in mass fraction. This might explain the flatness of the force-displacement curve for experiment CS00 which is very well captured by the model. The marked reduction of the horizontal force at higher levels of the displacement U might be due to softening effects induced in the masonry by the unreinforced mortar, an effect that is not captured by the ML model as presented here (see [Cardamone 2008] for a generalization of the model to softening and hardening behavior).

4D. *Masonry façade.* In this section we apply the ML material model to simulate the response of a simple two-story façade to working loads, seismic loads, and differential foundation subsiding. The geometry of the façade, the applied loads, and the boundary conditions are summarized in Figure 20. The façade is provided, above the openings, with 25 cm-thick wood beams and is assumed to be made of tuff and mortar of good quality. Wood is modeled as elastic with Young's modulus $E_w = 11$ GPa,
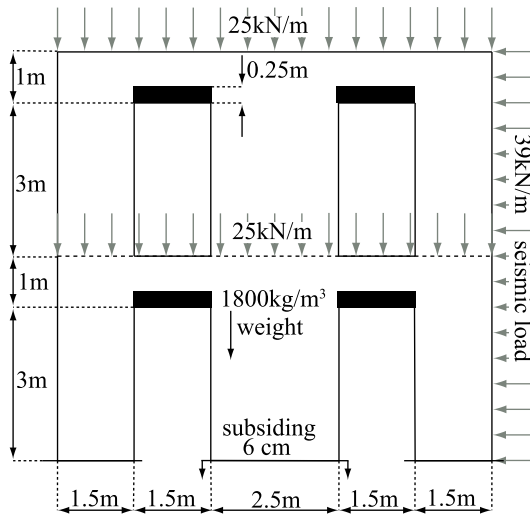

Figure 20. Masonry façade under working loads: geometry and load cases. Horizontal loads are considered in Section 4D2 and Figure 22, and foundation subsiding in Section 4D3 and Figure 24.
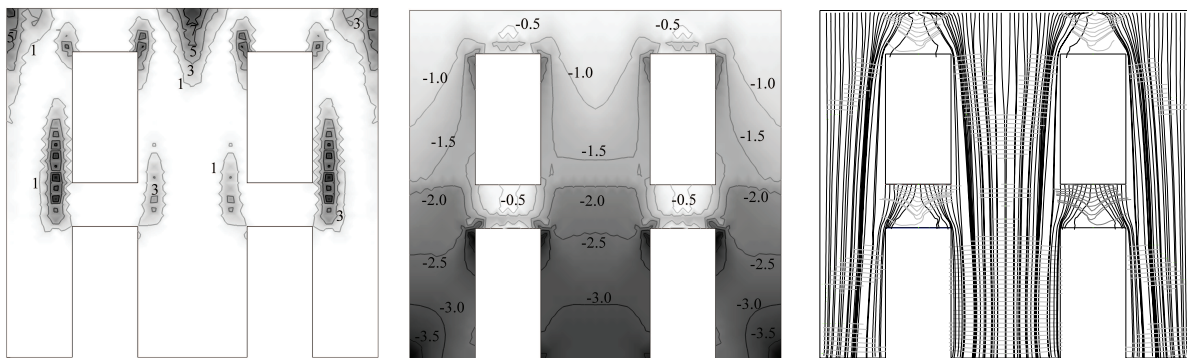
Figure 21. Masonry façade under working loads. Left: contour plot of the maximum fracture strain $[10^{-4}]$. Middle: contour plot of the maximum compressive stress $[10^5\,\text{Pa}]$. Right: isostatic lines of maximum and minimum stress (black and gray curves respectively).

Poisson's ratio $v_w = 0.35$, and density $\rho_w = 800\,\text{kg/m}^3$. For the tuff wall we assume Young's modulus $E = 660\,\text{MPa}$, Poisson's ratio $v = 0.2$, density $\rho = 1800\,\text{kg/m}^3$, and compression limit $\sigma_0 = 1.98\,\text{MPa}$. The whole structure is assumed to be 0.5 m thick.

4D1. *Working loads.* Working loads are represented by the weight of masonry and the force transmitted by the floors (25 kN/m); the results of the simulation are reported in Figure 21. The structure sustains the working loads without crushing. The value of the maximum stress at the base of the wall is about 0.35 MPa. The partition of the domain Ω can be inferred from Figure 21, right: $\boldsymbol{x} \in \Omega_1$ if both families of isostatics are defined, $\boldsymbol{x} \in \Omega_2$ if only the maximum compression isostatic is depicted, while $\boldsymbol{x} \in \Omega_3$ if the isostatics are not defined. In this load case we see that $\Omega_3 = \varnothing$ and $\Omega = \Omega_1 \cup \Omega_2$.

4D2. *Horizontal loads.* We simulated the response of the façade to a uniform force density of 39 kN/m distributed on the left side of the structure and superimposed on the structure subject to the working loads (see Figure 20). The total horizontal load is equivalent to 70% of the weight of the structure and is applied in ten steps. This kind of loading can be adopted to simulate seismic loads if horizontal ties or connections are present. Crushing strain accumulates in very localized regions near the corners (see Figure 22a). The formation of a compressed diagonal truss element is evident from Figures 22c and 22d. The force-displacement curve, depicted in Figure 23, shows that the structure is approaching collapse for the maximum horizontal load applied.

4D3. *Differential foundation subsiding.* A 6 cm subsiding is imposed, in fifteen steps, to the base of the central wall of the structure under working loads only. The structure shows peculiar kinematics, with the central wall following the foundation subsiding and the lateral walls rotating outward around the extremal points of the bases, where the plastic strain concentrates. The computed vertical component of the reaction of the central wall drops from about $3.9 \cdot 10^5$ N to $2.4 \cdot 10^5$ N after the subsiding. This computation suggests the redistribution of the vertical loads from the central to the lateral walls, redistribution that is also evident from the isostatics depicted in Figure 24d compared to the ones in Figure 21, right.
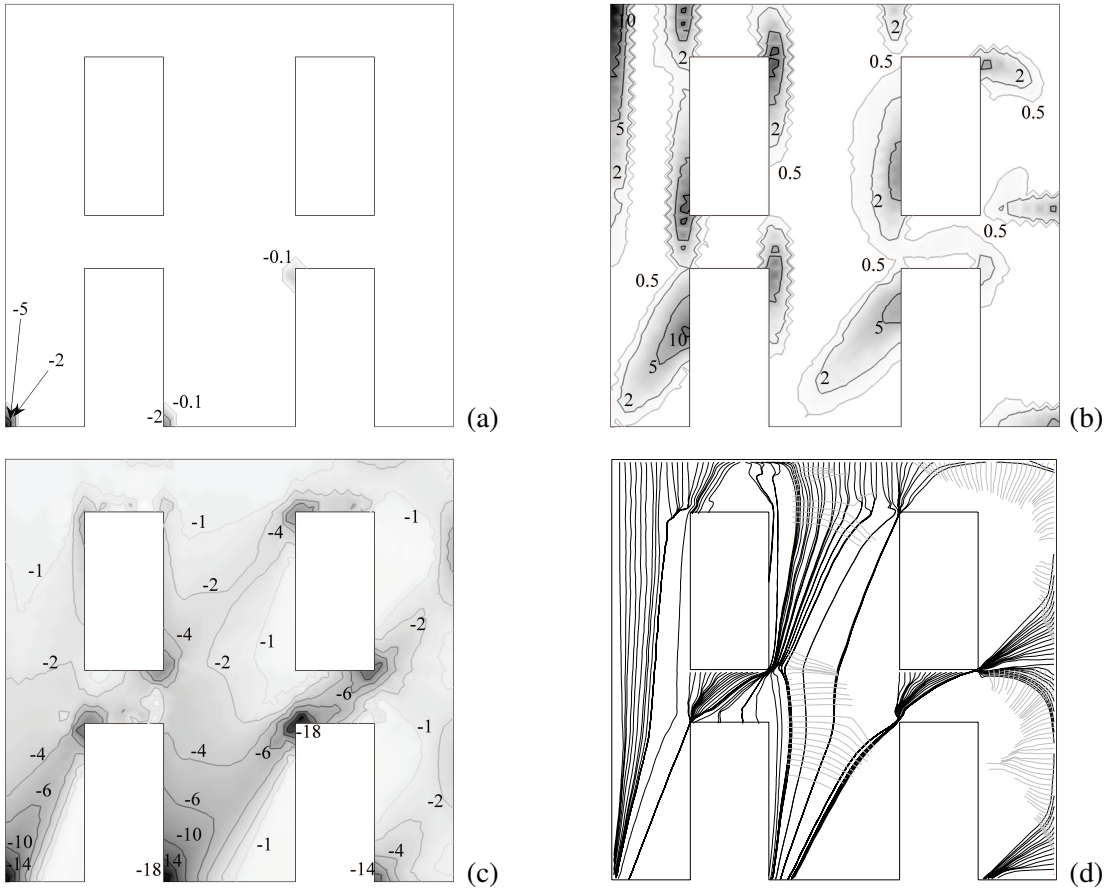
Figure 22. Masonry façade under working and horizontal loads: (a) contour plot of the maximum plastic strain $[10^{-4}]$, (b) contour plot of the maximum fracture strain $[10^{-3}]$, (c) contour plot of the maximum compressive stress $[10^5 \, \text{Pa}]$, and (d) isostatic lines of maximum and minimum stress (black and gray curves respectively).
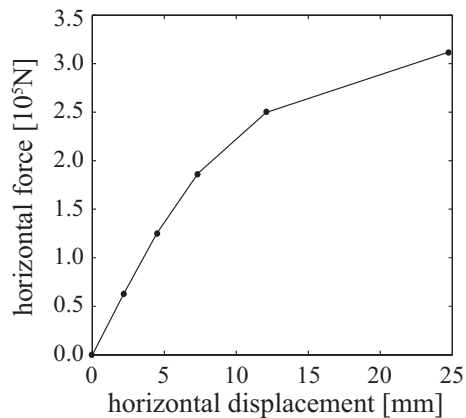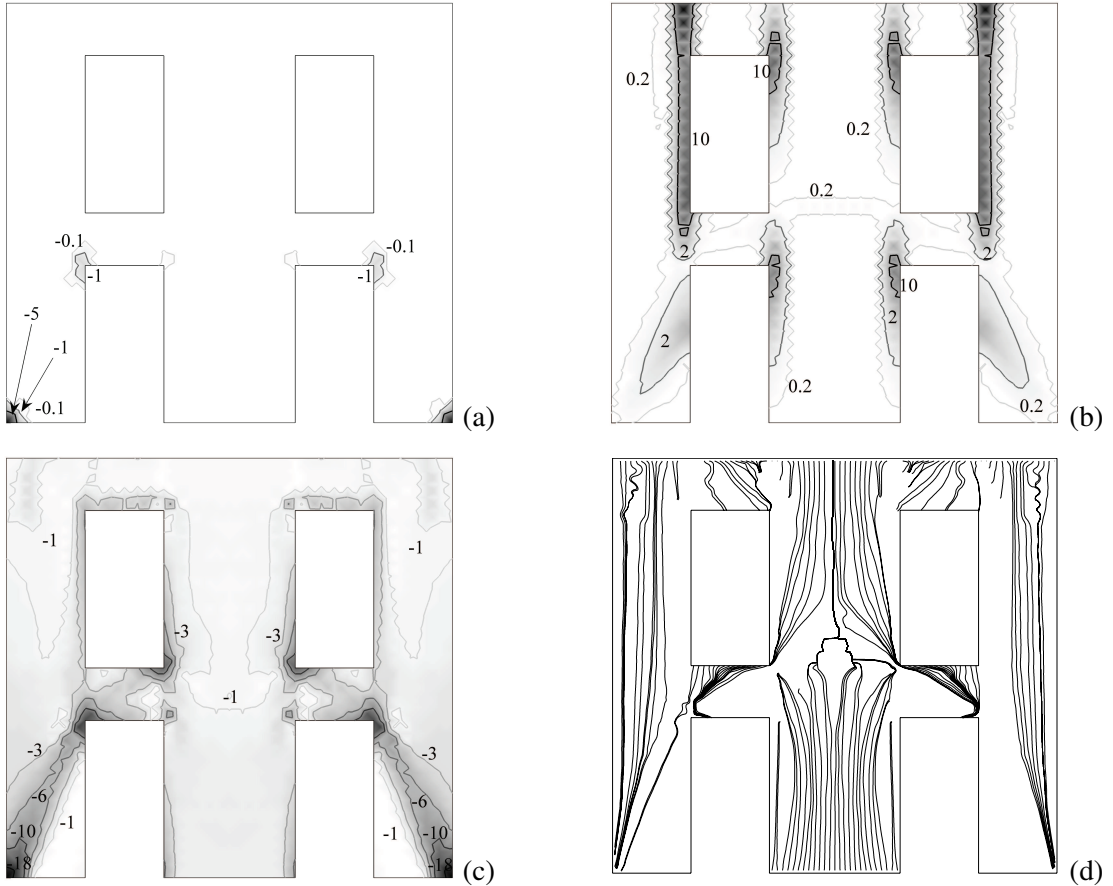

Figure 23. Masonry façade under working and horizontal loads (Figure 20): applied horizontal force versus leftward horizontal displacement of the midpoint of the top edge.

Figure 24. Masonry façade under working loads and foundation subsiding: (a) contour plot of the maximum plastic strain $[10^{-3}]$, (b) contour plot of the maximum fracture strain $[10^{-2}]$, (c) contour plot of the maximum compressive stress $[10^5 \, \text{Pa}]$, and (d) isostatic lines of maximum and minimum stress (black and gray curves respectively).

5. Conclusions

In the present paper we present a numerical FE model of masonry structures based on the normal elastic no-tension (NENT) and masonry-like material models.

The NENT material model is used extensively in the technical literature to model masonry materials. The attribute normal refers to a law of normality imposed on the total anelastic strain (fracture) to the cone N Sym of the admissible stress. It is essentially this assumption that makes the behavior of the material hyperelastic, allowing for a characterization of equilibrium states as minimizers of the total potential energy $\mathscr{E}(\boldsymbol{u})$.

A long debate on the physical feasibility of the normality assumption has agitated the research community working on masonry structures for decades. Is a fact that such an assumption is violated and manifestly false for macroscopically large fractures. The idea is that the normality assumption is close to reality at the onset of the cracking phenomenon and holds as long as fractures are small in size. Besides,

in real masonry structures, fractures appear and evolve in a completely different way: real macroscopic fractures open up through dissipation of a surface energy in an original coherent material. Often such fractures are preceded by microscopic cracks and voids through which the material is damaged and degraded, such cracks finally coalescing in a single macroscopic fracture.

Instead the model material is by assumption originally incapable of sustaining tensile stress. The law of normality on the latent strain has the effect, in rough terms, of giving some sort of fictitious coherence to the material, avoiding the sudden collapse of vertical walls under the action of feeble lateral forces.

Variational approximations based on the NENT model are supported by existence theorems only under rather restrictive assumptions on the loads. Many of the situations encountered in the applications (such as parts of the boundary subject to zero traction) are not covered by the known theorems. The function space in which the minimum problem can be formulated is rather wide and allows for discontinuous displacements.

The numerical model for the analysis of structures composed of NENT material that we propose is based on C^0 finite element triangulations. We apply it to several benchmark problems for which the known existence proofs do not work, detecting numerical convergence in all the cases considered and in particular linear convergence (the same expected in linear elasticity) and square root convergence for the cases of collapse loads and with strain singularities in the solution (not shown). The results we obtain encourage the adoption of continuous finite elements for the analysis of NENT materials.

As shown by the numerical examples we present, the stress level in masonry buildings can increase noticeably due to horizontal loads, differential subsidings, or geometrical modifications of the structure. As a matter of fact, in many cases of interest the collapse of a masonry structure is produced by simultaneous fracturing and crushing. The masonry-like (ML) model consists in the addition to the NENT model of a strength criterion for crushing consisting in a Prager–Drucker elastic-perfectly plastic yield criterion of the associated type.

The numerical strategy we adopt to solve the quasistatic evolution problem for ML materials is again based on energy minimization. The loading process is discretized into steps and the incremental solution at each step is obtained by minimizing a form of the energy updated step by step.

The desired convergence of the approximate trajectory to the exact one is proved in [Dal Maso et al. 2006] in the simpler case of elastic-perfectly plastic behavior.

In the numerical experiments we present, linear convergence is detected in the flexure problem. A number of more realistic examples solved with our FE code show how masonry structures are able to release high levels of stored elastic energy through sliding dissipation.

It has to be pointed out that the apparent sliding-type plasticity of our model simplifies more realistic dissipation phenomena due to friction. In the examples the release of elastic energy is not complete since unlimited ductility and softening effects are not taken into account.

Appendix A

As it is evident from Figure 2, the strain energy function φ characterizing NENT materials is not coercive. Mathematicians (see [Alfano et al. 2000; Angelillo et al. 2002] and references therein) restore coercivity of the total potential energy by considering the following load condition on the applied forces:

Supersafe load condition. The load $(\boldsymbol{p}, \boldsymbol{b})$ is said to be *supersafe* if there exists at least one stress field $\boldsymbol{T} \in \mathcal{H}$ such that $\boldsymbol{T} + \beta \boldsymbol{I} \in \mathrm{N}\,\mathrm{Sym}$ for some constant $\beta > 0$.

Here $\mathcal{H}$ is the set of statically admissible stress fields

$$\mathcal{H} = \{\boldsymbol{T} \in \mathcal{M}(\Omega) : \operatorname{div} \boldsymbol{T} + \boldsymbol{b} = \boldsymbol{0},\ \boldsymbol{T}\boldsymbol{n} = \boldsymbol{p} \text{ on } \partial\Omega_N,\ \boldsymbol{T} \in \mathrm{N}\,\mathrm{Sym}\}, \tag{A-1}$$

where $\mathcal{M}(\Omega)$ is a convenient Banach space. In other words the load is supersafe if there exists a stress field $\boldsymbol{T}$ that is strictly admissible over the open set Ω in a uniform way, that is, independently of $\boldsymbol{x}$. We prefer to give the name "safe load" to a load system $(\boldsymbol{p}, \boldsymbol{b})$ such that there exists a stress field that is strictly admissible over Ω, not necessarily in a uniform way, and add the attribute *super* to the load system that gives coercivity. If the load is safe then the potential energy associated with the external forces can be rewritten in the form

$$\int_{\partial\Omega_N} \boldsymbol{p} \cdot \boldsymbol{u}\,ds + \int_{\Omega} \boldsymbol{b} \cdot \boldsymbol{u}\,da = \int_{\Omega} \boldsymbol{T} \cdot (\boldsymbol{\varepsilon} + \boldsymbol{\lambda})\,da, \tag{A-2}$$

and the total potential energy becomes

$$\mathcal{E} = -\int_{\Omega} \boldsymbol{T} \cdot (\boldsymbol{\varepsilon} + \boldsymbol{\lambda})\,da + \frac{1}{2}\int_{\Omega} \boldsymbol{\varepsilon} \cdot \mathbb{A}^{-1}[\boldsymbol{\varepsilon}]. \tag{A-3}$$

Using the supersafe load assumption one can write

$$-\int_{\Omega} \boldsymbol{T} \cdot \boldsymbol{\lambda}\,da \geq \beta \int_{\Omega} |\boldsymbol{\lambda}|\,da; \tag{A-4}$$

then the energy has linear growth with respect to the norm of the space $BD(\Omega)$, that is, the space of functions $\boldsymbol{u}$ whose corresponding infinitesimal deformation is a bounded measure. For full information on this function space we refer to [Temam and Strang 1980]. Here we notice only that since the infinitesimal strain $\boldsymbol{e}$ is a bounded measure then $\boldsymbol{u}$ can be discontinuous and $\boldsymbol{e}$ can be decomposed into its absolutely continuous and singular parts with respect to two-dimensional Lebesgue measure:

$$\boldsymbol{e}(\boldsymbol{u}) = \boldsymbol{e}^a(\boldsymbol{u}) + \boldsymbol{e}^s(\boldsymbol{u}). \tag{A-5}$$

Recalling the decomposition of $\boldsymbol{e}$ into its elastic and fracture parts, since the potential energy depends quadratically on the elastic part of the deformation, only the fracture part $\boldsymbol{\lambda}$ can be singular, that is, only fracture discontinuities are admitted.

Theorem 6.8 of [Giaquinta and Giusti 1985, p. 381] shows the existence of the solution for the minimum problem (2-14) in $BD(\Omega)$ under the supersafe load condition and some supplementary technical conditions, in the special case of traction problems and isotropic elastic behavior. Since the energy is not strictly convex the solution is in general nonunique.

Also a dual energy principle based on the complementary energy can be considered. The stress state $\boldsymbol{T}^o$ that corresponds to the solution of the boundary value problem for NENT materials can be characterized as the minimizer of the energy functional

$$\mathcal{E}_c(\boldsymbol{T}) = -\int_{\partial\Omega_D} \boldsymbol{T}\boldsymbol{n} \cdot \bar{\boldsymbol{u}}\,ds + \frac{1}{2}\int_{\Omega} \boldsymbol{T} \cdot \mathbb{A}[\boldsymbol{T}], \tag{A-6}$$

over the set $\mathcal{H}$ of statically admissible stress fields [Giaquinta and Giusti 1985]. $\mathcal{M}(\Omega)$ in (A-1) can be considered as the Hilbert space $L^2(\Omega)$. In other words $\mathcal{H}$ is represented by the symmetric second order tensors $\boldsymbol{T}$ of $L^2(\Omega)$ such that $\boldsymbol{T}$ is negative semidefinite and balanced with $\boldsymbol{p}$ and $\boldsymbol{b}$. Obviously on considering $\boldsymbol{T}$ in $L^2(\Omega)$ the balance conditions must be considered in a generalized sense:

$$\int_\Omega \boldsymbol{T} \cdot \delta\boldsymbol{\varepsilon}\, da = \int_\Omega \boldsymbol{b} \cdot \delta\boldsymbol{u}\, da + \int_{\partial\Omega_N} \boldsymbol{p} \cdot \delta\boldsymbol{u} \quad \text{for } \delta\boldsymbol{u} \in \delta K, \tag{A-7}$$

where

$$\delta K = \{\delta\boldsymbol{u} \in H^1(\Omega) : \delta\boldsymbol{\varepsilon} = \tfrac{1}{2}(\nabla\delta\boldsymbol{u} + \nabla\delta\boldsymbol{u}^{\mathrm{T}}), \delta\boldsymbol{u} = \boldsymbol{0} \text{ on } \partial\Omega_D\}. \tag{A-8}$$

The choice of $L^2(\Omega)$ as the function space for the stress field is natural considering the quadratic term which represents the stress energy in $\mathcal{E}_c(\boldsymbol{T})$. Since the complementary energy functional is strictly convex over the convex set $\mathcal{H}$ the existence and the uniqueness of the minimizer $\boldsymbol{T}^{\mathrm{o}}$ of such a functional is guaranteed whenever $\mathcal{H}$ is not void (that is, there exists at least one stress field $\boldsymbol{T}$ such that $\boldsymbol{T}$ is negative semidefinite and balanced with $\boldsymbol{p}, \boldsymbol{b}$).

Therefore, though the solution $\boldsymbol{u}^{\mathrm{o}}$ may be nonunique, the elastic part $\boldsymbol{\varepsilon}^{\mathrm{o}}$ of the strain solution is unique. Nonuniqueness is restricted to the anelastic part of the deformation $\boldsymbol{\lambda}^{\mathrm{o}}$ and to special arrangements of the boundary conditions.

This circumstance makes the displacement and stress approach to the equilibrium of NENT materials nonsymmetric, in the sense that existence of the minimizer $\boldsymbol{T}^{\mathrm{o}}$ for $\mathcal{E}_c(\boldsymbol{T})$ is not sufficient for the existence of the minimizer $\boldsymbol{u}^{\mathrm{o}}$ of $\mathcal{E}(\boldsymbol{u})$. The existence of $\boldsymbol{T}^{\mathrm{o}}$ requires only the existence of an admissible stress field; the existence of $\boldsymbol{u}^{\mathrm{o}}$, with the known theorems, requires instead the existence of a uniformly strictly admissible stress field.

There are indeed counterexamples to the existence of $\boldsymbol{u}^{\mathrm{o}}$ in the case where the loads are admissible but do not satisfy the safe load condition. It has to be pointed out that the existence results obtained by mathematicians through the direct method of the calculus of variation are, from the engineering point of view, rather frustrating. Most of the buildings or masonry structures for which the stress and fracture fields are sought are under loads that are not supersafe since some part of the boundary is loaded with zero tractions.

To the authors knowledge there are no examples of nonexistence in the case in which the loads do not satisfy the supersafe load condition but there exists a balanced and strictly admissible stress field $\boldsymbol{T}$ (safe load). The only known counterexamples refer to the case in which the loads do not satisfy the supersafe load condition and there exists a balanced and admissible, but not strictly admissible, stress field $\boldsymbol{T}$. In the known counterexamples there are parts of the domain Ω that can be taken away without paying any energy price, that is, actually $|\boldsymbol{u}|_{BD} \to \infty$ and $\mathcal{E} = 0$; then we can say that the loads are collapse loads, in the sense that the deformation can increase indefinitely at constant load.

Another example of a collapse load is represented by the rocking mechanism of a wall. A homogeneous rectangular wall carrying its own weight is subject to increasing uniform horizontal forces pushing on the left edge of the wall. When the resultant of the vertical and horizontal forces passes through the bottom right vertex of the rectangle there exists a collapse mechanism for which $|\boldsymbol{u}|_{BD} \to \infty$ and $\mathcal{E} = 0$; then we can say that the loads are collapse loads, again in the sense that the deformation can increase indefinitely at constant load. In this second example balanced and admissible stress fields can be found that are not in $L^2(\Omega)$, $\boldsymbol{T}$ being only a bounded measure, e.g., a line Dirac delta.

Recently Lucchesi et al. [2008b] considered a number of examples referring to stress states that are bounded measures and statically admissible stress fields for safe loads and sometimes for collapse loads. The consideration of such concentrated stress fields is outside the scope of the present work, which is restricted to stress fields represented by symmetric second order tensors T belonging to $L^2(\Omega)$ such that T is negative semidefinite and balanced with p, b, and explicitly forbids the case of collapse loads. It has to be pointed out that numerical methods based on concentrated stress or strain have been recently proposed in the literature for the approximate solution of elastic problems (see for example [Davini and Pitacco 2000; Angelillo et al. 2002]) and could be extended to NENT or ML materials through relaxation of the energy $\mathcal{E}$.

Appendix B

In [Fortunato 2010], using the assumptions of the so-called TFT [Mansfield 1969], some analytical-numerical solutions are presented relative to rectangular panels made of NENT material undergoing arbitrary relative rigid displacements of the bases. This appendix summarizes the contents of that paper for the special case described in Section 3B.

Consider a rectangular ML panel, traction free on the lateral sides and subject to prescribed rigid body displacements of the top and bottom bases (Figure 25, left and middle). We introduce a Cartesian frame of reference $(O; x_1 = x, x_2 = y)$, with associated base vectors ($\hat{\boldsymbol{i}}$ and $\hat{\boldsymbol{j}}$), and define $\{u_A, v_A, \varphi_A\}$ as the translation and rotation parameters of the block $\mathcal{R}_A$ relative to pole A^0, $\{u_B, v_B, \varphi_B\}$ as the translation and rotation parameters of the block $\mathcal{R}_B$ relative to pole B^0, and $\{U, V, \Phi\}$ as the relative rigid displacement parameters between the top and bottom bases. The displacements of the top and bottom bases, modulo an ineffective rigid body translation, can be expressed in terms of the relative translation parameters. In the special case described in Section 3B we have

$$\boldsymbol{u}^a = U\hat{\boldsymbol{i}}, \quad \boldsymbol{u}^b = -U\hat{\boldsymbol{i}}. \tag{B-1}$$

Based on the complementary energy principle stated in Appendix A the equilibrium solution can be searched for by minimizing the energy (A-6) over the set $\mathcal{H}$ defined in (A-1). In particular we seek the solution in the restricted set $\tilde{\mathcal{H}}$ obtained by considering stress fields $T \in \mathcal{H}$ such that T is of rank one (the tension field assumption). The minimizer $\tilde{\boldsymbol{T}}$ of the complementary energy $\mathcal{E}_c$ over the restricted set $\tilde{\mathcal{H}}$ is generally an approximate solution of the BVP. For $T \in \tilde{\mathcal{H}}$ one has $\Omega = \Omega_2 \cup \Omega_3$, that is, $\Omega_1 = \varnothing$. Once the free boundary between Ω_2 and Ω_3 is localized, the solution of the equilibrium problem is reduced to the search for the stress field solution in Ω_2. In equilibrium and in the absence of body forces, in Ω_2 one of the two families of principal stress curves is made of straight lines that are called *compression rays* [Fortunato 2010]. The compression rays carry the nonzero stress and do not overlap. Since the lateral sides of the panel are stress free the compression rays intersect the boundary along the bases. Therefore the definition of the behavior of a single panel, under the above assumptions, is reduced to finding in Ω_2 the optimal compression ray distribution, the optimal choice being determined by energy convenience.

It is shown in [Fortunato 2010] that it is possible to locate the interfaces between the regions Ω_2 and Ω_3, in terms of the parameters $\{U, V, \Phi\}$, through geometrical arguments only. Such an interface is straight and along it the strain is zero, that is, the interface is an unextended ray. In the case of *pure shear* $\{U, 0, 0\}$ we have $\Omega = \Omega_2$ and $\Omega_3 = \varnothing$.
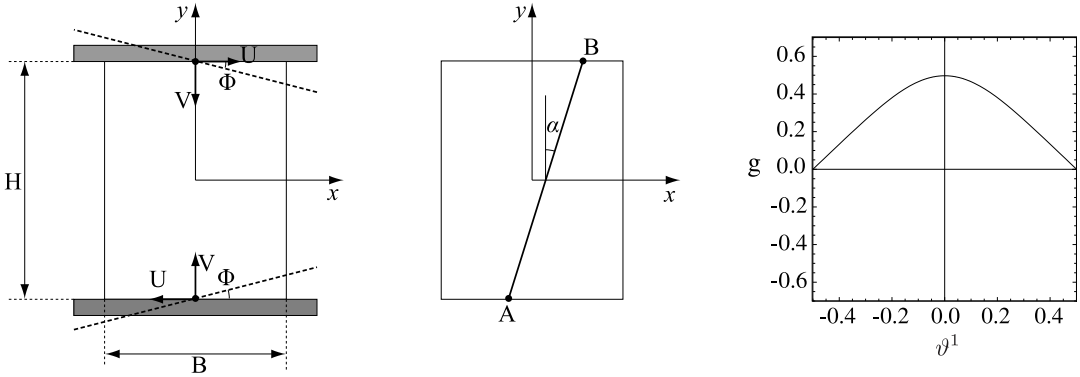
Figure 25. Left: panel geometry and relative displacements. Middle: typical ray geometry. Right: minimizer $g°$ for the problem described in Section 3B.

Given a rectangular panel of base B_0 and height H_0 we consider a *normalized* panel, that is, a rectangular panel whose bases are of unit length and whose height is $H = H_0/B_0$. We introduce the slope function g of a ray, that intersects the bottom and top bases at the abscissae x_A and x_B and the horizontal axis at $\vartheta^1 = (x_A + x_B)/2$, as follows:

$$\left[-\tfrac{1}{2}, \tfrac{1}{2}\right] \ni \vartheta^1 \mapsto g(\vartheta^1) := \tan\left(\alpha(\vartheta^1)\right), \tag{B-2}$$

where α is the angle between such a ray and the y axis as shown in Figure 25, middle. In order that the rays belong entirely to Ω, these geometrical constraints on g must be satisfied:

$$-\frac{1-2\vartheta^1}{H} \leq g(\vartheta^1) \leq \frac{1-2\vartheta^1}{H}, \quad \vartheta^1 > 0, \tag{B-3}$$

$$-\frac{1+2\vartheta^1}{H} \leq g(\vartheta^1) \leq \frac{1+2\vartheta^1}{H}, \quad \vartheta^1 \leq 0, \tag{B-4}$$

In Ω_2 it is convenient to introduce a system of curvilinear coordinates $(\vartheta^1, \vartheta^2)$ with one of the curvilinear lines, say ϑ^2, along the compression rays. In terms of the Cartesian coordinates $(x_1 \equiv x, x_2 \equiv y)$, with associated base vectors $(\hat{\imath}, \hat{\jmath})$, the curvilinear coordinates $(\vartheta^1, \vartheta^2)$ are defined by

$$x_1 = \vartheta^1 + g\vartheta^2, \quad x_2 = \vartheta^2, \tag{B-5}$$

where g, a function of ϑ^1 alone, is the slope of the rays defined in (B-2). Since in Ω_2 the stress is uniaxial along the direction of the compression ray, it admits the representation

$$\boldsymbol{T} = T^{22}\boldsymbol{a}_2 \otimes \boldsymbol{a}_2, \tag{B-6}$$

where $\boldsymbol{a}_2$ is one of the natural base vectors associated with the curvilinear coordinates system defined by (B-5).

The local equilibrium equations in Ω_2, in the absence of body forces and in terms of the curvilinear coordinates ϑ^1 and ϑ^2, gives

$$T^{22}{}_{,2} + T^{22}\frac{g'}{1 + g'\vartheta^2} = 0. \tag{B-7}$$

Therefore $\boldsymbol{T} \in \tilde{\mathcal{H}}$ if the only nonvanishing component of stress has the form

$$T^{22} = \frac{f}{1 + g'\vartheta^2}, \tag{B-8}$$

f being an arbitrary function of ϑ^1.

Assuming that the material has linear elastic isotropic behavior in compression and denoting by E and ν the Young's modulus and Poisson's ratio of the material, respectively, the complementary energy $\mathcal{E}_c$ can be written as

$$\mathcal{E}_c(f, g) = \int_{-1/2}^{1/2} f 2U \, d\vartheta^1 + \frac{1}{2} \int_{-1/2}^{1/2} \int_{H/2}^{H/2} \frac{1}{E} f^2 \frac{(1+g^2)^2}{1 + g'\vartheta^2} \, d\vartheta^1 d\vartheta^2. \tag{B-9}$$

$\mathcal{E}_c$ is a functional of the scalar functions f and g. These functions can be found by minimizing $\mathcal{E}_c$ with respect to f and g. We find f first. By taking the variation of $\mathcal{E}_c$ with respect to f one obtains the condition

$$\int_{-1/2}^{1/2} 2U \, d\vartheta^1 = -\int_{-1/2}^{1/2} \int_{H/2}^{H/2} \frac{1}{E} f^2 \frac{(1+g^2)^2}{1 + g'\vartheta^2} \, d\vartheta^1 d\vartheta^2, \tag{B-10}$$

that can be solved for f integrating the right hand side of (B-10) with respect to ϑ^2:

$$f = \frac{Eg'}{(1+g^2)^2} \frac{2Ug}{\ln(1 - g'H/2) - \ln(1 + g'H/2)}. \tag{B-11}$$

Substituting (B-11) into (B-9) and integrating with respect to ϑ^2, the complementary energy can be rewritten as

$$\mathcal{E}_c(g) = -2E \int_{-1/2}^{1/2} \frac{U^2 g'^2}{(1+g^2)^2 \ln \frac{1+g'H/2}{1-g'H/2}} \, d\vartheta^1. \tag{B-12}$$

Then minimizing $\mathcal{E}_c$ in $\tilde{\mathcal{H}}$ corresponds to maximizing the stress energy with respect to g.

We seek the minimum of the complementary energy functional among all functions g that satisfy the boundary conditions

$$g\left(-\tfrac{1}{2}\right) = 0 \quad \text{and} \quad g\left(\tfrac{1}{2}\right) = 0 \tag{B-13}$$

by finding the zeros of the *derivative* (the Euler equation) associated with (B-12):

$$\frac{8gU^2\left(6\gamma_1 g'^2(1 - g^2)(9g'^2 - 16) + 96g\gamma_2(\gamma_3 - \gamma_1)g''\right)}{\gamma_1^3 \gamma_2^3 (9g'^2 - 16)^2} = 0, \tag{B-14}$$

where

$$\gamma_1 := \ln \frac{1 + g'H/2}{1 - g''H/2}, \quad \gamma_2 := 1 + g^2, \quad \gamma_3 := Hg'.$$

The minimizer of $\mathcal{E}_c$, that is, the solution of the Euler equation, is actually unique and is denoted by g°. Observe that (B-14) can be simply solved numerically if the conditions are of *Cauchy* type. For the problem at hand boundary conditions are given, therefore to solve numerically (B-14) a *shooting*-type technique is adopted.

The solution g° for a rectangular panel of normalized lengths subject to given *shear* displacements $\{U, 0, 0\}$ is shown in Figure 25.

References

[Alfano et al. 2000] G. Alfano, L. Rosati, and N. Valoroso, "A numerical strategy for finite element analysis of no-tension materials", *Int. J. Numer. Methods Eng.* **48**:3 (2000), 317–350.

[Angelillo 1993] M. Angelillo, "Constitutive relations for no-tension materials", *Meccanica* (*Milano*) **28**:3 (1993), 195–202.

[Angelillo and Rosso 1995] M. Angelillo and F. Rosso, "On statically admissible stress fields for a plane masonry-like structure", *Quart. Appl. Math.* **53**:4 (1995), 731–751.

[Angelillo et al. 2002] M. Angelillo, A. Fortunato, and F. Fraternali, "A lumped stress method for plane elastic problems and the discrete-continuum approximation", *Int. J. Solids Struct.* **39**:25 (2002), 6211–6240.

[Angelillo et al. 2006] M. Angelillo, E. Babilio, and A. Fortunato, "Folding of thin walled tubes as a free gradient discontinuity problem", *J. Elasticity* **82**:3 (2006), 243–271.

[Angelillo et al. 2008] M. Angelillo, E. Babilio, L. Cardamone, and A. Fortunato, "A numerical model for variational fracture based on discontinuous finite elements", in *Proceedings of the 3rd Canadian Conference on Nonlinear Solid Mechanics* (*CanCNSM*) (Toronto, 2008), 2008.

[Angelillo et al. 2010] M. Angelillo, L. Cardamone, A. Fortunato, and M. Lippiello, "Descent strategies for finite element analysis of normal no-tension materials", preprint, 2010. Submitted to *Meccanica*.

[Benedetti and Steli 2008] A. Benedetti and E. Steli, "Analytical models for shear-displacement curves of unreinforced and FRP reinforced masonry panels", *Constr. Build. Mater.* **22**:3 (2008), 175–185.

[Benvenuto 1991] E. Benvenuto, *An introduction to the history of structural mechanics, II: Vaulted structures and elastic systems*, Springer, New York, 1991.

[Cardamone 2008] L. Cardamone, "Unilateral, elastoplastic behavior of masonry-like materials: some considerations on reinforcements application", in *Conference proceedings:* 7*th International PhD Symposium in Civil Engineering* (Stuttgart, 2008), edited by R. Eligehausen et al., Fédération Internationale du Béton/Institute of Construction Materials, Lausanne/Stuttgart, 2008.

[Castellano 1988] G. Castellano, "Un modello cinematico per i materiali non resistente a trazione", pp. 241–256 in *Cinquantenario della Facoltà di Architettura di Napoli: Franco Jossa e la sua opera*, edited by U. Carputi, Istituto di Costruzioni, Facoltà di Architettura, Napoli, 1988.

[Como 1992] M. Como, "Equilibrium and collapse analysis of masonry bodies", *Meccanica* (*Milano*) **27**:3 (1992), 185–194.

[Como and Grimaldi 1985] M. Como and A. Grimaldi, "A unilateral model for the limit analysis of masonry walls", pp. 25–45 in *Unilateral problems in structural analysis*, edited by G. Del Piero and F. Maceri, CISM Courses and Lectures **288**, Springer, Vienna, 1985.

[Dal Maso et al. 2006] G. Dal Maso, A. DeSimone, and M. G. Mora, "Quasistatic evolution problems for linearly elastic-perfectly plastic materials", *Arch. Ration. Mech. An.* **180**:2 (2006), 237–291.

[Davini and Pitacco 2000] C. Davini and I. Pitacco, "An unconstrained mixed method for the biharmonic problem", *SIAM J. Numer. Anal.* **38**:3 (2000), 820–836.

[De Giorgi 1996] E. De Giorgi, "Congetture riguardanti alcuni problemi di evoluzione", *Duke Math. J.* **81**:2 (1996), 255–268.

[Del Piero 1989] G. Del Piero, "Constitutive equation and compatibility of the external loads for linear elastic masonry-like materials", *Meccanica* (*Milano*) **24**:3 (1989), 150–162.

[Di Pasquale 1984] S. Di Pasquale, "Questioni concernenti la meccanica dei mezzi non reagenti a trazione", pp. 227–238 in *Atti del VII Congresso Nazionale AIMETA, 5: Meccanica delle strutture* (Trieste, 1984), Associazione Italiana de Meccanica Teorica ed Applicata, Milano, 1984.

[Eucentre 2008] Eucentre, "Prove murature", 2008, Available at http://www.eucentre.it/provemurature.

[Fortunato 2010] A. Fortunato, "Elastic solutions for masonry-like panels", *J. Elasticity* **98**:1 (2010), 87–110.

[Giaquinta and Giusti 1985] M. Giaquinta and E. Giusti, "Researches on the equilibrium of masonry structures", *Arch. Ration. Mech. An.* **88**:4 (1985), 359–392.

[Heyman 1995] J. Heyman, *The stone skeleton: structural engineering of masonry architecture*, Cambridge University Press, 1995.

[Lucchesi et al. 1996] M. Lucchesi, C. Padovani, and N. Zani, "Masonry-like solids with bounded compressive strength", *Int. J. Solids Struct.* **33**:14 (1996), 1961–1994.

[Lucchesi et al. 2008a] M. Lucchesi, C. Padovani, G. Pasquinelli, and N. Zani, *Masonry constructions: mechanical models and numerical applications*, Lecture Notes in Applied and Computational Mechanics **39**, Springer, Berlin, 2008.

[Lucchesi et al. 2008b] M. Lucchesi, M. Šilhavý, and N. Zani, "Integration of measures and admissible stress fields for masonry bodies", *J. Mech. Mater. Struct.* **3**:4 (2008), 675–696.

[Luciano and Sacco 1997] R. Luciano and E. Sacco, "Homogenization technique and damage model for old masonry material", *Int. J. Solids Struct.* **34**:24 (1997), 3191–3208.

[Mansfield 1969] E. H. Mansfield, "Tension field theory", pp. 305–320 in *Applied mechanics: proceedings of the 12th International Congress of Applied Mechanics* (Stanford, CA, 1968), edited by M. Hetényi and W. G. Vincenti, Springer, Berlin, 1969.

[Marfia and Sacco 2005] S. Marfia and E. Sacco, "Numerical procedure for elasto-plastic no-tension model", *Int. J. Comput. Methods Eng. Sci. Mech.* **6**:3 (2005), 187–199.

[Mielke and Ortiz 2008] A. Mielke and M. Ortiz, "A class of minimum principles for characterizing the trajectories and the relaxation of dissipative systems", *ESAIM Control Optim. Calc. Var.* **14**:3 (2008), 494–516.

[Ortiz and Simo 1986] M. Ortiz and J. C. Simo, "An analysis of a new class of integration algorithms for elastoplastic constitutive relations", *Int. J. Numer. Methods Eng.* **23**:3 (1986), 353–366.

[Romano and Romano 1979] G. Romano and M. Romano, "Sulla soluzione di problemi strutturali in presenza di legami costitutivi unilaterali", *Rend. Accad. Naz. Lincei* **67** (1979), 104–113.

[Romano and Sacco 1984] G. Romano and E. Sacco, "Sul calcolo di strutture non resistenti a trazione", pp. 221–233 in *Atti del VII Congresso Nazionale AIMETA* (Trieste, 1984), Associazione Italiana de Meccanica Teorica ed Applicata, Milano, 1984.

[Sab 2003] K. Sab, "Yield design of thin periodic plates by a homogenization technique and an application to masonry walls", *C. R. Mécanique* **331**:9 (2003), 641–646.

[Temam and Strang 1980] R. Temam and G. Strang, "Functions of bounded deformation", *Arch. Ration. Mech. An.* **75**:1 (1980), 7–21.

MAURIZIO ANGELILLO: mangelil@unisa.it
University of Salerno, Via Ponte Don Melillo, 84084 Fisciano, Italy

LUCA CARDAMONE: lcardamo@unisa.it
University of Salerno, Via Ponte Don Melillo, 84084 Fisciano, Italy

ANTONIO FORTUNATO: a.fortunato@unisa.it
University of Salerno, Via Ponte Don Melillo, 84084 Fisciano, Italy

JOURNAL OF MECHANICS OF MATERIALS AND STRUCTURES

Journal of Mechanics of Materials and Structures